Ocean Engineering 342 (2025) 122718

Contents lists available at ScienceDirect

Ocean Engineering

journal homepage: www.elsevier.com/locate/oceaneng

Research paper

A 6-DOF submarine manoeuvrability prediction code - Part I: Development and validation

Lorenzo Berté [a,*], Diego Villa [a], Michele Viviani [a], Giorgio Mazzarello [b], Francesco Carmone [b], Benedetto Piaggio [a]

[a] Dept. of Naval Architecture – DITEN, University of Genoa, Genoa, 16145, Italy
[b] Fincantieri DMM, Genoa, 16129, Italy

ARTICLE INFO

Keywords:
Submarines
Underwater vehicles
Manoeuvrability
Stern planes
Rudder
Hydrodynamics
Control and stability

ABSTRACT

A software that accurately predicts submarine manoeuvring behaviour is essential for hull, sail and control surfaces design. In this context, the availability of a reliable 6-DOF parametric, modular, and robust model is highly advantageous at early design-stage. The here presented mathematical model is based on strip theory for calculating the linear forces on the bare hull, combined with non-linear cross-flow drag forces. The contribution of control surfaces and the sail are evaluated using a formulation derived from experiments and literature data, allowing to consider the specific geometry of the exposed surfaces and the hull sections on which they are mounted, thus including all mutual interaction effects between the various components, such as the body-wing and wing-body. In this first part of work a comparison between the results of the manoeuvring code and experimental data or other data available in literature is presented, demonstrating satisfactory reliability and robustness with a view to estimating stability and controllability.

1. Introduction

The hydrodynamics governing submarine manoeuvrability are substantially more complex than those of surface vessels, owing to the involvement of six degrees of freedom (6-DoF) and the dependence of stability and control characteristics on vessel speed. In contrast to surface ships, submarines operate in both horizontal and vertical planes, with a longitudinal restoring moment that remains independent of speed. This increased complexity introduces significant challenges in maintaining trim and depth control, which are further compounded by hydrodynamic interactions among the bow appendages, sail, and stern planes. One particularly notable phenomenon is stern dipping (Bridges et al., 2003), wherein vortices shed from the sail induce out-of-plane forces that cause the stern to pitch downwards (Spencer, 1968), (Bridges et al., 2003). These interactions necessitate an integrated theoretical and experimental approach to submarine design.

Safe and effective submarine operation (ABS, 2002; Kirikbaş and Şakir, 2021) requires accurate manoeuvrability prediction tools and a reliable simulation framework for control system development. A modular hydrodynamic methodology permits the independent evaluation of forces generated by the hull, sail, propeller, and control surfaces while capturing their mutual interactions. Early-stage predictions of stability and controllability characteristics are essential for refining hull geometries and optimising control surface configurations prior to final design decisions. This study presents a mathematical model capable of predicting the hydrodynamic forces acting on a submarine, enabling the simulation of manoeuvres such as turning circles in the horizontal plane, zig-zag tests in both planes and depth-change manoeuvres.

While considerable progress has been made in manoeuvring prediction for surface vessels (Sutulo et al., 2002), (Perez et al., 2004), (ABKOWITZ, 1964), and other model such as Ankudinov et al. (1993), Hooft et al. (1994), Carchen et al. (2020), and Yoshimura (2005), Li et al. (2022), the body of literature addressing submarine manoeuvring remains comparatively limited, primarily due to industrial and military restrictions on experimental data dissemination. Nevertheless, existing submarine manoeuvring models generally follow the same foundational principles as those for surface ships, with extensions to incorporate full 6-DoF dynamics (Renilson, 2015; Ovalle et al., 2011).

A key distinction lies in the configuration of the control surfaces: submarines typically employ four aft appendages and two forward planes to achieve control in both vertical and horizontal planes. Determining hydrodynamic force and moment coefficients is essential for accurate manoeuvring simulations. These coefficients may be derived from experimental fluid dynamics (EFD), computational fluid dynamics (CFD), or semi-empirical formulations. Established mathematical models, such as those proposed by Gertler and Hagen (1967), Feldman (1995), Kim et al.

* Corresponding author.
E-mail address: lorenzo.berte@edu.unige.it (L. Berté).

https://doi.org/10.1016/j.oceaneng.2025.122718
Received 18 December 2024; Received in revised form 11 July 2025; Accepted 3 September 2025
Available online 4 October 2025

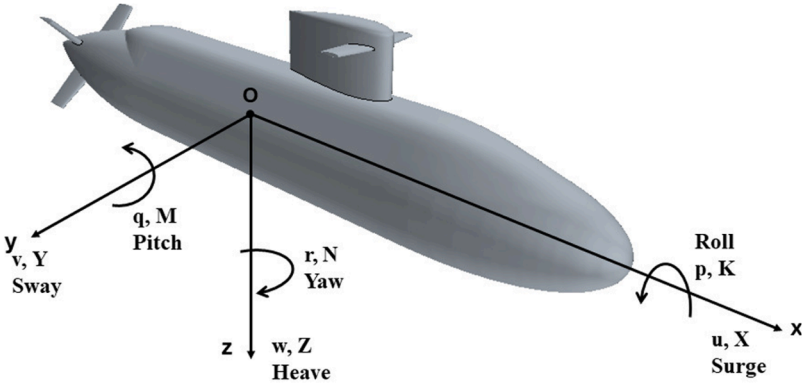

Fig. 1. Coordinate system.

(2023), Renilson and Renilson (2018), adopt a six-degree-of-freedom (6-DoF) framework incorporating specific coupling terms between the manoeuvring planes. The present study builds upon previous research (Piaggio et al., 2022b; Gaggero et al., 2022), further enhancing and extending existing models through additional investigations (Zheku et al., 2023) aimed at optimising simulator performance.

1.1. DITEN approach

The here presented mathematical model is both modular and parametric in structure. The modular approach enables independent evaluation of the forces and moments generated by each hydrodynamic component - hull, sail, and control surfaces, followed by an integrated assessment that considers their mutual interactions, including the amplification of control surface effectiveness due to hull mounting, the interaction between sail-induced vortices and the hull - i.e., the stern dipping phenomenon. The model framework combines slender-body theory and lifting-surface theory with semi-empirical, numerical, and experimental data, ensuring both reliability and robustness. In parallel to this semiempirical model, an alternative one is present, i.e. the CEFD (Computational Experimental Fluid Dynamics). This model is based on (Gertler and Hagen, 1967). In this case, the CEFD model differs from the DITEN approach in that it requires precomputed hydrodynamic coefficients-obtained via CFD or EFD-as input. By contrast, the DITEN model internally estimates these coefficients using semi-empirical formulations combined with strip theory.

A benchmark fleet of five submarines is employed to validate the model. Three of these-SUBOFF (Liu and Huang, 1998), Swe (Thuné, 2015), and BB2 (Overpelt et al., n.d.; Joubert, 2004)-have fully documented geometries, while the remaining two, SUB+ and SUBX, are subject to industrial confidentiality constraints. These case studies encompass a diverse range of hull forms, sail placements, and control surface configurations, enabling a comprehensive assessment of submarine hydrodynamic performance. To the authors' knowledge, no prior comparative study has analysed and published five submarine configurations with significantly different geometries, incorporating a broad spectrum of manoeuvres, time histories, and hydrodynamic coefficients. The manoeuvring characteristics of the vessels are compared with available free running experimental data or captive model testing based models CEFD.

The first phase of the study is devoted to validating the simulator against experimental data. Standard manoevures, including Turning circle and horizontal e vertical zigzag, are simulated and compared with experimental data available in leterature. At a second stage, Planar Motion Mechanism (PMM) tests in 6-DoF are used to have a further insight into the problem, considering BB2 and SUB+, with DITEN-estimated hydrodynamic coefficients compared to experimental values where available.

One of the principal aims of this work is to demonstrate the reliability of the semi empirical DITEN model across a wide dataset of submarine designs, including experimental data for both cruciform and X-configuration control surfaces. It has to be underlined that the quality of available experimental data varies considerably; unfortunately, it is not possible to properly assess the reliability of each considered test case, nevertheless, it is believed that the broad analysis carried out allows to capture the overall trends.

Once the reliability and robustness of the proposed simulator are established, the future second part of the present study will focus on a detailed parametric investigation. Simulations will be performed to evaluate the effects of systematic variations in rudder dimensions, appendage geometries, and hull forms. Additional analyses based on numerical methods will be also conducted to further refine the model and explore in greater detail how hull shape and control surface design influence manoeuvring behaviour.

1.2. Paper outline

Section 3 describes the five case studies. Section 4 presents the mathematical framework embedded within the simulator, covering modelling strategies for the hull, sail, appendages, and interaction effects. Section 5 validates the simulator by comparing its predictions with experimental results and reporting the global mean error. Finally, Section 6 summarises the key findings and outlines potential directions for future work.

2. Submarine reference system

In this study, a body-fixed coordinate system describes the submarine's motion, as shown in Fig. 1. The origin of the coordinate system (denoted as (o)) is positioned at the mid-body along the shaft axis. The coordinates are defined within a right-handed coordinate system, with the x- and y-axes lying in the horizontal plane. The x-axis is positive toward the bow, while the y-axis is positive toward the starboard; consequently, the z-axis is vertical, with positive values directed downward. The velocities u, v, and w represent surge, sway, and heave, respectively, while p, q, and r represent roll, pitch, and yaw angular velocities. Six hydrodynamic forces acting on the submarine: the longitudinal force X along the x-axis, the lateral force Y along the y-axis, the vertical force Z along the z-axis, the roll moment K around the x-axis, the pitch moment M around the y-axis, and the yaw moment N around the z-axis.

3. Case study

The selected case study fleet exhibits substantial design variations, as illustrated in Fig. 2, encompassing a wide range of hull forms and geometric configurations. Each case is supported by a comprehensive

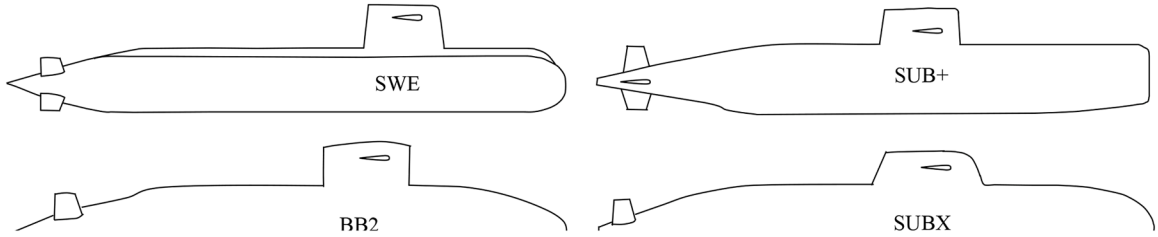

Fig. 2. Case study.

Table 1
Test cases characteristics.

Vessel	L/B	B/D	LCG/L	$\frac{A_H^{long}}{LD}$	$\frac{A_H^{top}}{LB}$	$\frac{A_S}{A_H}$	$\frac{x_S}{L}$	$\frac{A_s}{A_H}$	$\frac{x_s}{L}$	$\frac{A_b}{A_H}$	$\frac{x_b}{L}$
SUBOFF	8.575	1.000	0.035	0.83	0.83	3%	5.1	3.8%	0.40	0%	0
SWE	10.048	0.729	0.058	0.81	0.90	11%	7.5	5.1%	0.42	1.2%	0.22
BB2	7.313	0.906	0.027	0.83	0.85	7%	7.5	6.4%	0.37	1.5%	0.19
SUB+	9.619	0.820	0.096	0.80	0.81	7%	6.3	5.3%	0.41	1.4%	0.13
SUBX	7.986	0.814	0.054	0.85	0.83	9%	5.7	4.7%	0.45	1.3%	0.13

dataset, including experimental results from free-running trials and hydrodynamic coefficients obtained from towing tank experiments. In the following, the different vessels are briefly described. In Table 1, the main geometric parameters of each vessel are reported.

1. **SUBOFF**, is a model-scale research submarine from Defence Advanced Research Projects Agency (DARPA) SUBOFF project at the David Taylor Research Centre, Groves et al. (1989), where captive model tests have been carried out. The simple vehicle geometry is widely acknowledged to be unrealistic (the fairwater is too small, the hull is a simple revolution body, and it has small stern planes and no bow control surfaces). The stern planes are mounted in a +-configuration. The SUBOFF is unstable in both the vertical and horizontal planes of manoeuvre, due to its specific geometric characteristics. This instability makes it a particularly relevant case study for evaluating the extent and robustness of the software. Unfortunately, no free running model tests are available and only a few simulations of manoeuvres have been carried out on the basis of CFD calculations; the results are also largely dispersed, probably because of the large instability of the vessel. For this case study is available a set of hydrodynamics coefficients (Roddy, 1990; do Nascimento and Tannuri, 2020). For this vessel the following manoeuvres are available: simulations with TC10, TC35, and ZZ10h.
2. **SWE**, is a demo submarine from the Swedish navy (Thuné, 2015), with X-configuration rudder design, and a modern shaped sail. Results of captive and free-running tests are available even if there is no reference; it is not clear if these data are obtained simply by simulations or experimental tests. A complete set of hydrodynamic coefficients is available for this case study in the horizontal plane; furthermore, an incomplete set of coefficients in the vertical plane is available. For this vessel the following IMO manoeuvres are available: simulations involving TC20, ZZ10h, and ZZ05v.
3. **BB2** submarine. The BB2 is a modern SSK-class underwater vehicle based on the concept design by Joubert (Joubert, 2004, 2006). The BB2 submarine features a modern-shaped sail, and X-configuration of stern control surfaces. The casing is integrated longitudinally with the hull, extending from the bow to the beginning of the stern cone. The keel structure is completely absent. The geometric shape of the sail is similar to that of the SWE vessel, featuring a streamlined design but without specific fillets where it intersects with the hull. For this model, free-running model tests are available upon request from MARIN. Additionally, a set of hydrodynamic coefficients and simulations by Kim et al. (2023) are available for this case study. However, the simulations conducted by Kim et al. (2023) cover only manoeuvres in the horizontal plane, excluding the vertical plane interactions. For this vessel the following IMO manoeuvres are available : TC15, TC20, TC30, ZZ10h, ZZ20h, ZZ05v, and ZZ10v.
4. **SUB+**, the geometry of this vessel is confidential. The control surfaces are mounted into a +-configuration, i.e. a traditional design. The sail is less integrated on the hull, lacking fillets. The keel structure is integrated into the hull and extends from the bow to the stern cone. The upper platform is also integrated into the hull, running from the bow to the aft end, with a notable narrowing in the bow region. A set of coefficients obtained from experimental PMM model tests are available for this vessel. This is the only test case with a complete set of coefficients for both the manoeuvring planes, inclusive of some free running experimental data. Although the geometry of this vessel is not modern, it remains a fundamental test case due to the quality of the available experimental and simulated data. Furthermore, it is the only non-literature vessel available featuring a traditional +-configuration. For this vessel the following IMO manoeuvres are available: TC10, TC20, TC35, and ZZ5v.
5. **SUBx** Also for this vessel the geometry is confidential. This is a modern submarine class prototype with an X-plane. The keel structure is not aligned with the hull, extending longitudinally from approximately 70% of hull from the aft perpendicular. The upper platform is partially aligned in the transverse plane, with a curvature discontinuity at the intersection with the hull. The sail geometry is more modern than the $SUB+$ case, featuring a tapered design smoothly integrated with the upper platform at the front. The sail height is reduced compared to the other configurations. Hydrodynamic coefficients for this submarine are available, although these coefficients are incomplete in the vertical plane. For this vessel the following IMO manoeuvres are available: TC10, TC20, TC30, and TC35.

In the Table 1 a summary of fleet details is provided, with an eye on the *hull* main ratios (subscript H), the sizing and positioning of the *sail* (subscript S) and *control surfaces* along the hull (subscript s stands for the stern planes and rudders, while b for bow planes). Accordingly: A_S, A_s and A_b are the respective areas; x_S, x_s and x_b the longitudinal coordinates. Finally, A_H^{long} and A_H^{top} are the longitudinal and top-view projected areas of the hull.

In Table 2 a summary of available reference data for each submarine is provided, if captive or free-running, if experimental or numerical.

4. Mathematical models

As already mentioned, two models are available to predict manoeuvring behaviour:

Table 2
Table of available vessel data.

Vessel	Captive EXP	Captive NUM	Manoeuvring SIM	manoeuvring EXP-Free Running
SWE	✓	X	✓	X
SUBOFF	✓	X	✓	X
BB2	✓	✓	✓	✓
SUB+	✓	X	✓	✓
SUBX	✓	X	✓	✓

- A model developed in-house by DITEN, referred as the DITEN model
- A model developed according to Gertler and Feldman (Feldman, 1995; Gertler and Hagen, 1967), exploiting data, in terms of hydrodynamic coefficients, coming from captive tests, both from CFD simulations or from experiments, called CEFD model. The hydrodynamic forces and moments equations of the CEFD model are reported in Appendix A.

The two models differ in the computation of hydrodynamic and control surface forces. All other forces, including propeller forces, resistance, and inertial forces, are evaluated using the same methodologies, and the equations of motion are solved using the same approaches in both models.

4.1. Equations-of-motion

The six degrees of freedom equations of motion are derived by Newton's second law and are previously presented by Abkowitz (ABKOWITZ, 1964).

$$M\left[\dot{u} - vr + wq - x_G\left(q^2 + r^2\right) + y_G\left(pq - \dot{r}\right) + z_G\left(pr + \dot{q}\right)\right] + X\dot{m} = X_{\text{HYDRO}} \tag{1a}$$

$$M\left[\dot{v} - wp + ur - y_G\left(r^2 + p^2\right) + z_G\left(qr - \dot{p}\right) + x_G\left(qp + \dot{r}\right)\right] + Y\dot{m} = Y_{\text{HYDRO}} \tag{1b}$$

$$M\left[\dot{w} - uq + vp - z_G\left(p^2 + q^2\right) + x_G\left(rp - \dot{q}\right) + y_G\left(rq + \dot{p}\right)\right] + Z\dot{m} = Z_{\text{HYDRO}} \tag{1c}$$

$$I_x\dot{p} + (I_z - I_y)qr - (\dot{r} + pq)I_{zx} + (r^2 - q^2)I_{yz} + (pr - \dot{q})I_{xy} + M\left[y_G(\dot{w} - uq + vp) - z_G(\dot{v} - wp + ur)\right] + K\dot{m} = K_{\text{HYDRO}} + K_{\text{BG}} \tag{1d}$$

$$I_y\dot{q} + (I_x - I_z)rp - (\dot{p} + qr)I_{xy} + (p^2 - r^2)I_{zx} + (qp - \dot{r})I_{yz} + M\left[z_G(\dot{u} - vr + wq) - x_G(\dot{w} - uq + vp)\right] + M\dot{m} = M_{\text{HYDRO}} + M_{\text{BG}} \tag{1e}$$

$$I_z\dot{r} + (I_y - I_x)pq - (\dot{q} + rp)I_{yz} + (q^2 - p^2)I_{xy} + (rq - \dot{p})I_{zx} + M\left[x_G(\dot{v} - wp + ur) - y_G(\dot{u} - vr + wq)\right] + N\dot{m} = N_{\text{HYDRO}} \tag{1f}$$

where: K_{BG} and M_{BG} are the transverse and longitudinal righting moments, (ρ) is the density of water; $(I_{xx}, I_{zz}, I_{xz}, I_{zx})$ are the moments of inertia;(x_G) is the longitudinal coordinate of the center of gravity with respect to the midship perpendicular, m is the mass of the ship.

In the next subsections the modular modelling of each component of the submarine is outlined.

4.2. Hull

The mathematical model of the bare hull includes the main hull + keel structure + the deck structure. The forces acting on them are evaluated by means of a strip-theory approach (Clarke, 1972; Hooft et al., 1994) . This model is based on a sectional hull formulation that considers the sectional shape distribution from bow to stern, including keel and deck structures, i.e. the hydrodynamic hull. The manoeuvring forces are divided into a linear component and a non-linear viscous contribution. The linear component is based on the strip theory for slender bodies with a correction for three-dimensional effects. The non-linear viscous contribution is evaluated using cross-flow drag theory as fostered by Clarke (1972), Bohlmann (1990).

$$X'_{\text{H}} = X'_{vr} \cdot v'^2 \cdot r' + X'_{wq} \cdot w'^2 \cdot q' + R'_T(u) \tag{2a}$$

$$Y'_{\text{H}} = Y'_{uv} \cdot u'^2 \cdot v' + Y'_{ur} \cdot u' \cdot r' + Y'_{up} \cdot u' \cdot p' + Y'_{\text{nl}} \tag{2b}$$

$$Z'_{\text{H}} = Z'_{uw} \cdot u'^2 \cdot w' + Z'_{uq} \cdot u' \cdot q' + Z'_{\text{nl}} + Z'^{S}_{H} \tag{2c}$$

$$K'_{\text{H}} = K'_{v} \cdot u'^2 \cdot v' + K'_{r} \cdot u' \cdot r' + K'_{up} \cdot |u'| \cdot p' + K'_{\text{nl}} \tag{2d}$$

$$M'_{\text{H}} = M'_{uw} \cdot u'^2 \cdot w' + M'_{uq} \cdot u' \cdot q' + M'_{\text{nl}} + M'^{S}_{H} \tag{2e}$$

$$N'_{\text{H}} = N'_{uv} \cdot u'^2 \cdot v' + N'_{ur} \cdot u' \cdot r' + N'_{up} \cdot u' \cdot p' + N'_{\text{nl}} \tag{2f}$$

where:

- $u' = \frac{u}{\sqrt{u^2+v^2+w^2}}$, $v' = \frac{v}{\sqrt{u^2+v^2}}$, $w' = \frac{w}{\sqrt{u^2+w^2}}$, $p' = \frac{p}{\sqrt{u^2+v^2+w^2}}L$, $q' = \frac{q}{\sqrt{u^2+w^2}}L$, $r' = \frac{r}{\sqrt{u^2+v^2}}L$
- X'_{vr} and X'_{wq} are the hydrodynamic coefficients in X in dimensionless form, calculated through regression (Sutulo et al., 2002). In this case, no alternative formulations using *strip theory* are available.
- $Y'_{uv}, Y'_{ur}, N'_{uv}, N'_{ur}$ are the linear hydrodynamic coefficients in v and r, in dimensionless form, calculated by integrating the sectional added mass.
- $Z'_{uw}, Z'_{uq}, M'_{uw}, M_{uq}$ are the linear hydrodynamic coefficients in w and q, in dimensionless form, calculated by integrating the sectional added mass.
- $Y'_{\text{nl}}, Z'_{\text{nl}}, M'_{\text{nl}}, N'_{\text{nl}}$ represent the non-linear contributions of lateral force and moment, calculated using the *cross-flow drag* theory.
- Z'^{S}_{H} and M'^{S}_{H} are the *stern dipping* coefficients due to the interaction between the sail and the hull, with the formulation detailed in the dedicated Section 4.7.
- $K'_{uv}, K_{ur}, K'_{\text{nl}}$ are the coefficients used to evaluate the heeling moment derived from the lateral forces provided by $Y'_{uv}, Y'_{ur}, Y'_{\text{nl}}$, vertically centred at the hydrodynamic centre of volume.
- $K'_{up} = -2\xi_\phi(u)\sqrt{I'_{xx} - K'_{\dot{p}}}\frac{\Delta BG}{V^2}$ is the roll damping coefficient.
- $R'_T(u)$ represents the hydrodynamic resistance of the submarine.

The main advantage of the approach is that it considers the actual shape of the hull with the sectional shape along the length and not only the main dimensions of the hull. For instance, it avoids the limitations of the equivalent ellipsoid in Munk's theory (Munk, 1924) adopted by Pattison (1975) - where only a destabilizing moment, known as the Munk moment, is evaluated.

In Fig. 3, an example of the sectional technique is provided, which enables the evaluation of force distribution along the hull in response to a lateral drift velocity, similar to Bohlmann (1990): using slender-body theory for linear terms and crossflow-drag theory for non-linear terms. In the next subsections, some details of the methodologies are reported, respectively.

4.2.1. Strip-theory - hull linear contributions

The calculation of the linear coefficients is performed by integrating the distribution of sectional added masses in the longitudinal direction, $m_{yy}(\xi)$ and $m_{zz}(\xi)$, respectively, in the horizontal and vertical planes of manoeuvre. This integration begins from the evaluation of the added mass for 2D sections, calculated using the following expressions, according to a longitudinal coordinate ξ, originating at the bow and directed towards the stern:

$$m_{yy}(\xi) = \frac{1}{2}\rho\pi H^2(\xi)C_H(\xi) \tag{3}$$

$$m_{zz}(\xi) = \frac{1}{2}\rho\pi B^2(\xi)C_V(\xi) \tag{4}$$

Where: $H(\xi)$ section height, $B(\xi)$: section beam, sectional added mass coefficient.

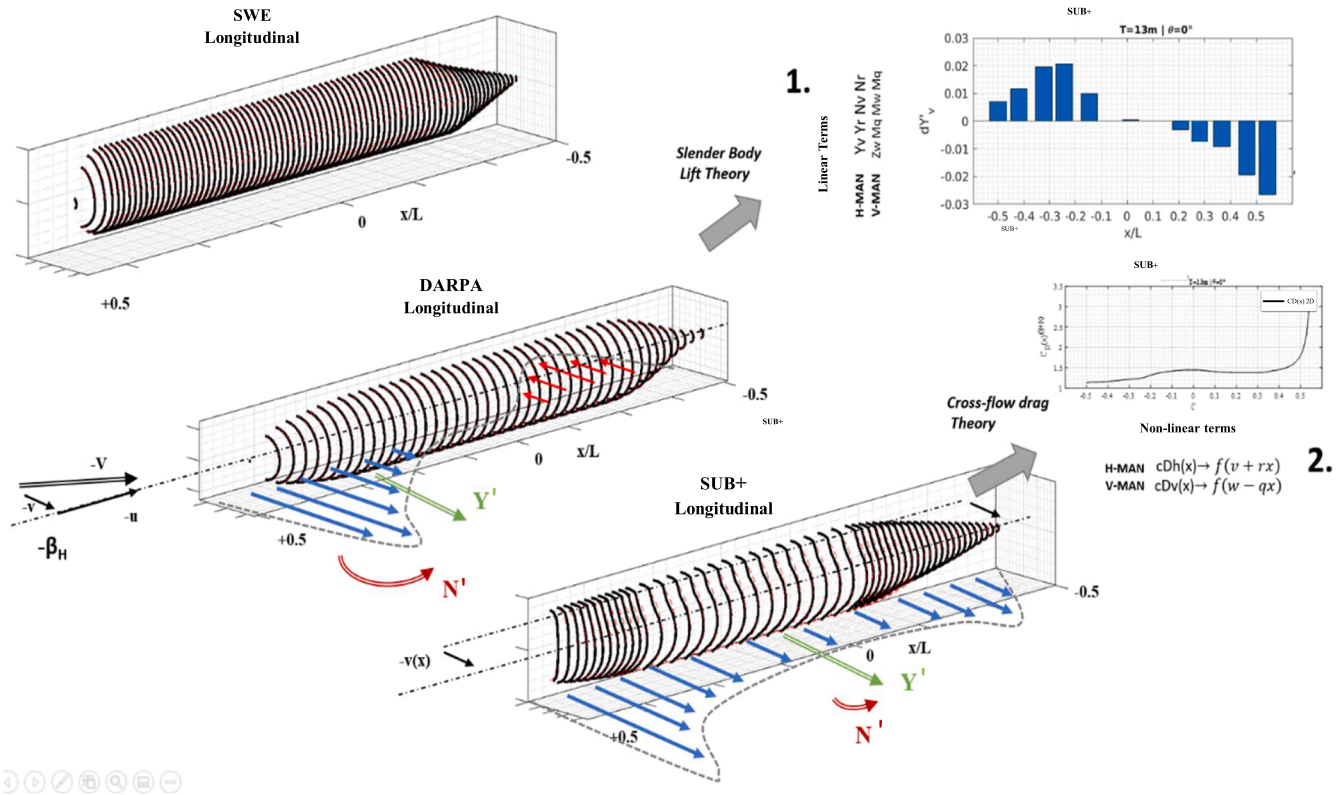

Fig. 3. Bare hull-example of strip theory sectional forces.

The sectional added masses are evaluated adopting a semi-empirical approach based on the section's geometric characteristics (width, draft/height, and fineness coefficient) (Piaggio et al., 2022b). Afterwards, by applying appropriate viscous corrections for the stern distribution of added mass , the method results in a corrected 3D distribution, M_{yy}, inclusive of boundary layer thickness development and separation at stern end - for details see (Toxopeus, 2008). Finally, the linear coefficients are obtained by integrating along the ship's length (Clarke, 1972), according to the following equations:

$$Y_{\dot{v}} = -\int_{\text{stern}}^{\text{bow}} M_{yy}^{uv}\, dx, \quad N_{\dot{v}} = -\int_{\text{stern}}^{\text{bow}} x M_{yy}^{uv}\, dx \tag{5}$$

$$Y_{\dot{r}} = -\int_{\text{stern}}^{\text{bow}} M_{yy}^{ur}\, dx, \quad N_{\dot{r}} = -\int_{\text{stern}}^{\text{bow}} x M_{yy}^{ur}\, dx \tag{6}$$

$$Y_{uv} = -M_{yy}^{uv}\Big|_{\text{stern}}, \quad Y_{ur} = -M_{yy}^{ur}\Big|_{\text{stern}} \tag{7}$$

$$N_{uv} = -\left[M_{yy}^{uv}\Big|_{\text{stern}} + \int_{\text{stern}}^{\text{bow}} M_{yy}^{uv}\, dx \right] \tag{8}$$

$$N_{ur} = -\left[x M_{yy}^{ur}\Big|_{\text{stern}} + \int_{\text{stern}}^{\text{bow}} M_{yy}^{ur}\, dx \right] \tag{9}$$

In analogy, the same coefficients are evaluated in the vertical plane, dependent on the accelerations ($Z_{\dot{w}}$, $M_{\dot{w}}$, $Z_{\dot{q}}$, $M_{\dot{q}}$) and the velocities (Z_{uw}, M_{uw}, Z_{uq}, M_{uq}), by directly integrating the added masses. Vice-versa, the longitudinal added masses are assessed according to a semi-empirical formulation, Eq. (10):

$$X_{\dot{u}} = \left(0.4466\left(\frac{L}{B}\right)^{-1.235}\right)\left(\frac{4}{3}\rho\pi\left(\frac{L}{2}\right)\left(\frac{B}{2}\right)^2\right) \tag{10}$$

The bare hull added mass due to the roll ($K_{\dot{p}}$) is considered negligible in comparison to the subsequent contributions from appendages and is therefore excluded from the present study.

4.2.2. Cross-flow drag - hull non-linear contributions: Bluff body drag

Non-linear force contributions are crucial for broader kinematics, particularly in scenarios involving tighter manoeuvres and high drift angles. The non-linear component of lateral \vertical forces and yaw \pitch moments, whether due to pure drift, pure rotation, or a combination of drift and rotational speeds, is calculated as a function of the local transverse and vertical incident velocities, referred to as "cross-flow". Accordingly, on the horizontal and vertical planes, the following equations are obtained:

$$v(x) = v + r \cdot x, \quad w(x) = w - q \cdot x \tag{11}$$

Consequently, the forces result from the integration along the length of the hull of the sectional contributions. For instance, on the horizontal plane, this is expressed as follows:

$$Y_{\text{nl}} = -0.5\rho \int_{\text{stern}}^{\text{bow}} C_D(x)\, v(x)\, |v(x)|\, h(x)\, dx, \tag{12}$$

$$N_{\text{nl}} = -0.5\rho \int_{\text{stern}}^{\text{bow}} C_D(x)\, v(x)\, |v(x)|\, h(x)\, x\, dx \tag{13}$$

where $C_D(x)$ is the distribution of the sectional cross-flow drag coefficient, evaluated using empirical formulations for two-dimensional drift. This coefficient depends on B/H and C_X, where B and H represent the local width and height of the hull (bare hull, keel, and deck), respectively, while C_X is the sectional coefficient.

4.3. Propeller

The propeller model exploits four-quadrant curves in terms of C_t and C_q, given the standard design thrust K_t and torque K_q curves as a function of the advance ratio $J = \frac{u_A}{nD}$. An additional formulation for the lateral force $K_S = \frac{S}{\rho n^2 D^4}$ was included to encompass the unbalancing of tangential forces along the blade revolution in oblique flow.

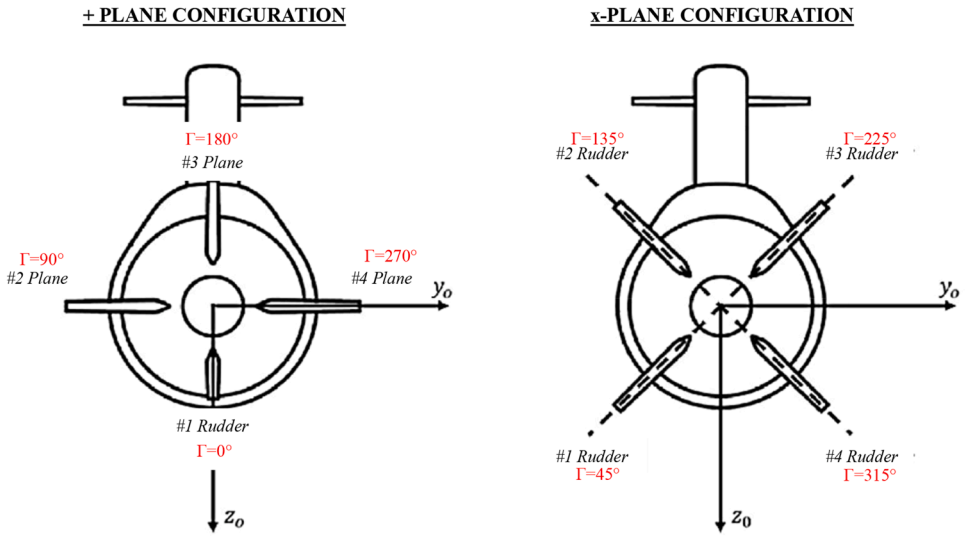

Fig. 4. Stern appendages standard configurations.

According to Dubbioso et al. (2013), a linear coefficient including the cross-flow velocity was obtained at propeller plane, counteracting the stern sidestep speed analogously in both the vertical and horizontal planes:

$$\frac{\partial K_S}{\partial v'} = K_{Sv}, \tag{14}$$

$$K_{Sv} = 2.12J\left(K_Q - \frac{J}{2}\frac{dK_q}{dJ}\right) \tag{15}$$

This term is needed for very unstable submarines since it is the only term that is able to counteract the yaw/pitch motions when the stern control surfaces are self-aligned to the local inflow once the rotation has been triggered.

4.4. Control planes and appendages

The four aft control surfaces are numbered from 1 to 4, starting from the lower surface and proceeding clockwise when viewed from the bow, as illustrated in Fig. 4. This numbering system ensures that each surface is uniquely identified, regardless of the configuration employed, starting from the first down-pointing surface.

To study the inflow velocities at each appendages, both fixed and movable, the reference velocities at their respective centres of pressure along the quarter-chord are considered. For this purpose, several local reference frames have been introduced, rotated by the installation angle Γ relative to the longitudinal axis (0° when oriented downward). An example of this is illustrated by the inflow velocities at the rudders (subscript R), as shown in Fig. 5.

The reference systems of the generic considered rudder, as illustrated in Fig. 5, are as follows:

- $[P_R : u_R, v_R, w_R]$, $local - ref$ - A local reference centred at the centre of pressure of the appendage and parallel to the reference of the hull, which includes the components of induced velocity due to the rotational motions of the submarine;
- $[P_R : c_o, t_o, s_o]$,$rud - ref$ - A reference fixed to the closed appendage, rotated by an installation angle Γ around u_R. The reference individuates the sectional blade reference along the chord, in the thickness-wise, and span-wise out direction;
- $[P_R : d, \ell, s_o]$,$inflow - ref$ - A reference aligned with the inflow velocity at the appendage,which is rotated by a local drift angle β around the previous s_o axis. The reference individuates the lift and drag components and their direction of action.

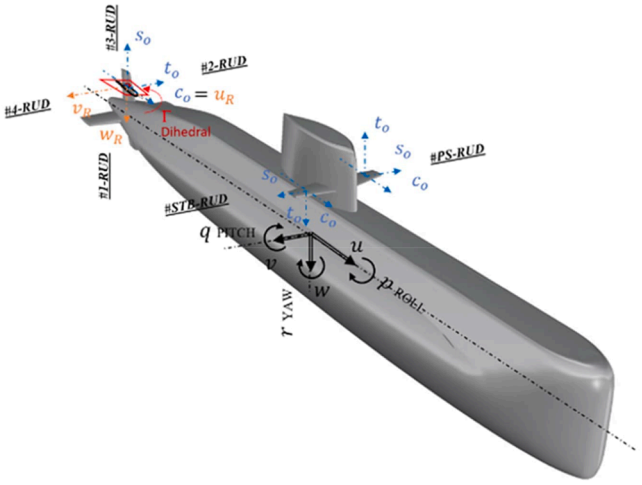

Fig. 5. Reference system-velocity on stern rudders.

In particular, starting from the velocities concerning the hull reference frame (orange frame in Fig. 5), the induced velocities are added, taking into account the effect of hull straightening.

The coefficients C_l and C_d are evaluated from data available in various literature sources (Feldman, 1995; Piaggio et al., 2022a; Whicker and Fehlner, 1958; Windsor, 1962; Thieme, 1965; Molland and Turnock, 2007; Viviani et al., 2014), depending on the blade geometric characteristics and mounting type onto the hull.

Within the code, it is possible to define the type of rudder installed on the vessel, allowing for selecting a fully-movable spade, or partially movable of skeg and horn types. Some rudder configurations include a fixed portion of the appendage along the chord and span directions, referred to as the *Skeg* and *Head Box*, respectively shown in Fig. 9.

The mathematical equations describe the behaviour of the appendage, distinguishing between the contributions of the rudder with a zero deflection angle of the movable part (in terms of stability) and the movable portion deflected (in terms of control). The fixed portion is subjected to an angle of attack δ_{Re}, while the movable part is subjected to an angle of attack α_{fe}. Thus, the following definitions are written:

$$\alpha_{fe} = \alpha_f - \beta_R \tag{16}$$

$$\delta_{Re} = -\beta_R \tag{17}$$

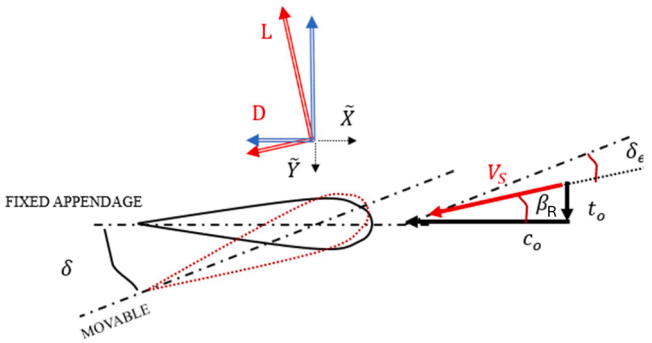

Fig. 6. Reference system-velocity on section of stern rudders.

Given the angles of attack, the movable and fixed components of lift and drag forces can be obtained according to the following equations:

$$C_L = C_L^{\text{mov}}(\alpha_{fe}) + C_L^{\text{fix}}(\delta_{Re}) \tag{18}$$

$$C_D = C_{Do}(\alpha_{fe}) + C_L^2 \cdot \frac{1}{e\pi \cdot ar_e} \tag{19}$$

with

$$C_L^{\text{mov}} = K \frac{\partial C_L}{\partial \delta} \sin \alpha_{fe} \cos^{\zeta} \alpha_{fe} \tag{20}$$

$$C_L^{\text{fix}} = (1-K) \frac{\partial C_L}{\partial \delta} \delta \cdot \sigma(\delta) \tag{21}$$

where K is a coefficient that differentiates between movable and fixed elements, as explaned below $\frac{\partial C_L}{\partial \alpha}$ and $\frac{\partial C_L}{\partial \delta_{Re}}$ represent the partial slope of lift with respect to the movable and fixed parts; the trigonometric expression $\cos^{\zeta} \alpha_{fe}$ and the sigmoid function $\sigma(\delta_{Re})$ include the stalling behaviours of the lifting surfaces, after separation; $C_{D0}(\alpha_{fe})$ is the zero angle viscous drag of the appendage; e, is the Oswald efficiency which takes into account of the finite span efficiency of the lift induced drag component – i.e. a correction factor that represents the change in drag with lift of a three-dimensional wing, as compared with an ideal wing having the same aspect ratio and an elliptical lift distribution.

In detail: the coefficient K takes into account of eventual presence of a *skeg* which reduces the movable part in the chord direction – by means of the chord ratio c_f/c, or the presence of a *head box*, which reduces the movable part in the span direction – according to the span ratio s_f/s. The lift slope of the movable part, against the fully movable appendage, is evaluated according to the AEW formulation (Pattison, 1975; Pitts et al., 1959) shown in Fig. 7: on the left side due to the skeg presence $K^{SK}(c_f/c)$, on the right side due to the headbox presence $K^{HB}(s_f/s)$. According to these factors $K = K^{SK} \cdot K^{HB}$. For instance, without a fixed appendage portion, i.e. fully-movable spade control surface, K equals 1, resulting in no reduction.

Overall, the modelled lift and drag characteristics can be schematized according to the following sketch – Fig. 8: the lift curve C_L with closed movable part, is characterised by split piece-wise linear formulation by varying δ_e, respectively relying onto the stall and peak max lift angles; on the other hand, by varying the angle of the movable part α_{fe}, the same curves result in a shift at $\delta_e = 0$. In particular, the slope of the linear segment $\frac{\partial C_L}{\partial \delta}$, as well as the positioning of the stall angles α_{stall} and peak angle α_{peak}, follows semi-empirical formulations based on the aspect ratio, the hull's taper ratio, the sweep angle, and the tip shape (square or rounded). At high angles, lift stall is represented by a sigmoid function $\sigma(\delta_e)$, which smoothly connects the final segment of the curve to zero. On the other hand, the linear slope in the direction of the movable part angle follows $\frac{\partial C_L}{\partial \alpha}$, and stalls based on the trigonometric formulations and its power ζ.

The drag curve C_D follows a quadratic formulation for the induced component by lift, in the initial segment, starting from the viscous and pressure drag at zero angle C_{D0}. At larger angles, the formulation transitions to the pure effect of cross-flow drag cC_{FD} as a function of the taper ratio, parallelly to the loss of lift performance. The transition between the two operational modes is linear.

4.5. Hydrodynamic interactions

To evaluate interactions with the hull, the DITEN mathematical model employs the AEW philosophy (Pattison, 1975) to include the wing increase of effectiveness (body-on-wing) and hull amplification (wing-on-body). This approach accounts for wing-body interaction, capturing the increase in the effectiveness of the control surfaces at zero deflection angle (stability) and the performance degradation of the rudder at non-zero deflection angles (control) due to the reduction of the aspect ratio of the exposed portion only.

The model starts from the study of pair of appendages installed on the hull's elliptical section of radius r, as illustrated in Fig. 9 i.e. the double body full wing theory, with symmetry plane the dash-dotted line. The geometric span is defined as the height of the *exposed half wing* s. In contrast, the effective span of the *full extended wing* is defined as the total extension between the tips of the two symmetrically installed profiles, identified as b in Fig. 9: $s_e = \frac{b}{2} = r + s$ where r is the radial distance between the hull's centreline and the intersection point between the hull and the rudder.

From the exposed area of the control surface $A_g = cs$ and the geometric aspect ratio $ar_g = \frac{b^2}{A_g}$, the lift and drag characteristics are derived

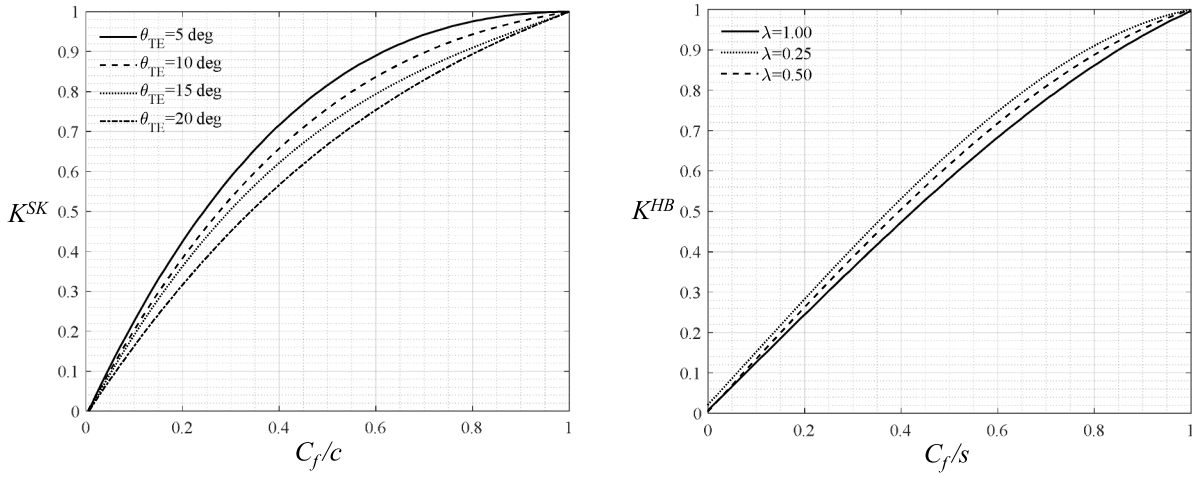

Fig. 7. Chord-wise extent and trailing edge angle (θ_{TE}). Span-wise extent and taper ratio (λ).

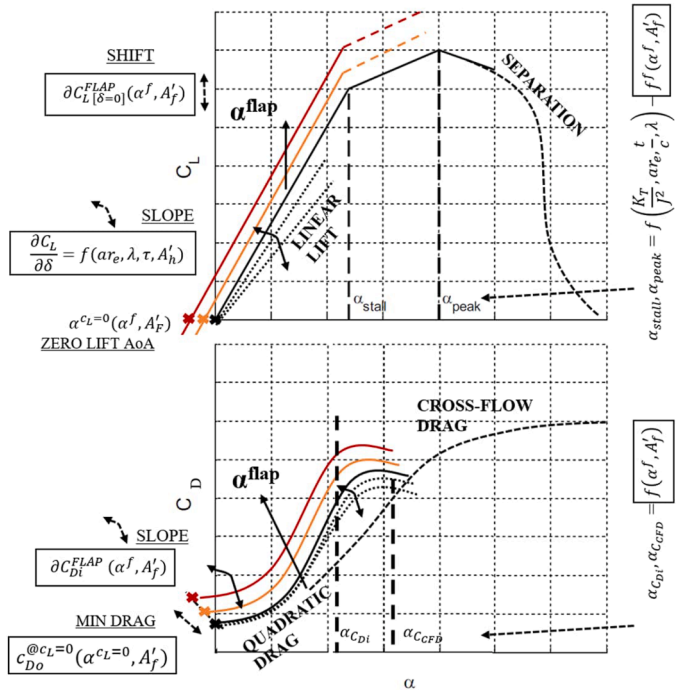

Fig. 8. DITEN model characteristic rudder curves.

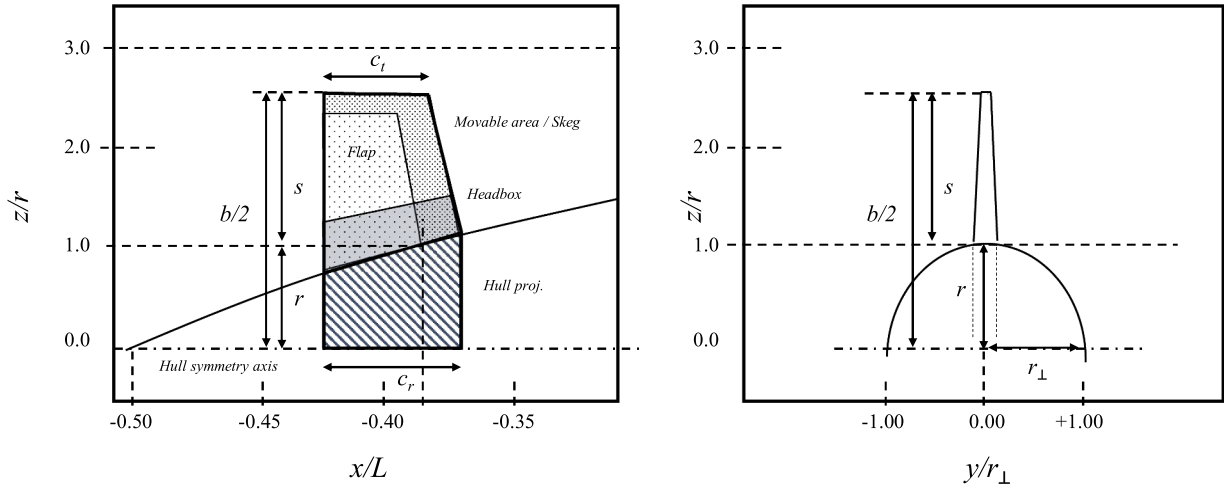

Fig. 9. Geometric parameters of the control surface.

in terms of the effective quantities of the extended wing: $A_e = A + c_r r$ and $ar_e = (s + r)^2/A_e$, which include the trunk of cone in-between.

Starting from the extended wing, a reduction factor must be applied to the lift curve due to the fact that the hull is not a lifting surface, but a slender body. Corrections are considered separately for stability and controllability to correct the effective aspect ratio of the mirrored and extended wing.

For *stability*, the interactions are included in the coefficients $K_b(w)^*$ and $K_w(b)^*$ (Pitts et al., 1959), as depicted in Fig. 10, according to the following equation, which starts from the extended wing lift slope $\frac{dC_L^{ext}}{d\delta}$:

$$\frac{dC_L}{d\delta} = \frac{dC_L^{ext}}{d\delta}[K_b(w)) + K_w(b)]^* \tag{22}$$

For *controllability*, a loss of effectiveness is evaluated due to the gap at the root of the rudders in the case of fully movable fins. This loss is represented by two terms analogous to $k_b(w)$ and $k_w(b)$ (Pitts et al., 1959), as illustrated in Fig. 11, starting from the lift slope in stability:

$$\frac{dC_L}{d\alpha_f} = \frac{dC_L}{d\delta}\frac{k_b(w) + k_w(b)}{K_b(w) + K_w(b)} \tag{23}$$

For partially movable fins, finally, repartition Eqs. (20) and (21) apply, consequently to headbox and skeg sizing, according to the descending K factors.

Additional effects, such as the sail vortex shedding, and hull shielding onto the stern planes, are included as straightening factors which modify the inflow velocity and local drift angles onto the surfaces as in the next section – for details see (Bertè et al., 2025).

4.6. Inflow kinematics of fixed and movable appendages

The submarine velocity vector is locally translated into the centre of pressure coordinates of the fin $[x_R, y_R, z_R]^T$ and the vehicle angular

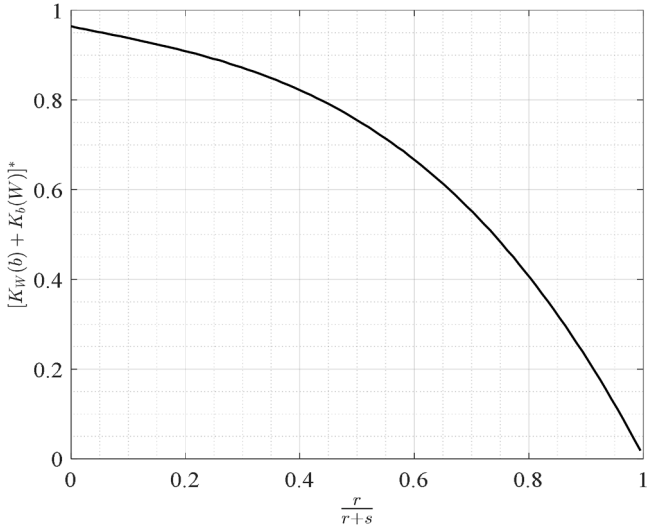

Fig. 10. Stern control surface-stability loss due to fins at the tail end of hulls with respect to the full-span equivalent wing.

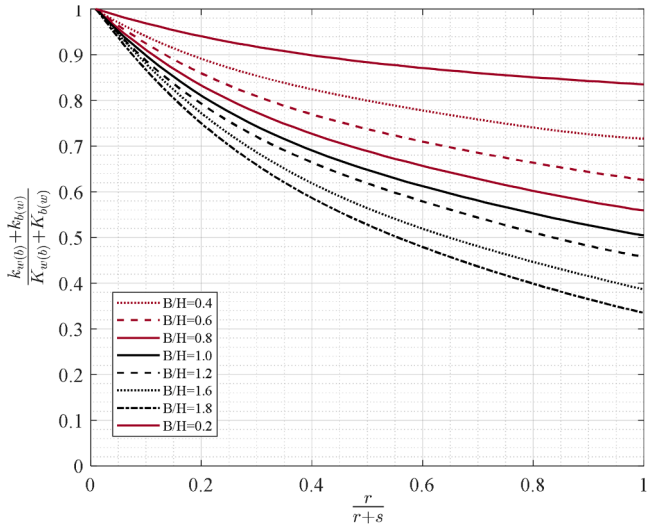

Fig. 11. Control surface over stability contribution for elliptical sections.

velocities, according to the following – see Fig. 5:

$$\begin{bmatrix} u_R \\ v_R \\ w_R \end{bmatrix} = \begin{bmatrix} \gamma_u \cdot u \\ \gamma_v \cdot v \\ \gamma_w \cdot w \end{bmatrix} + \begin{bmatrix} \gamma_p \cdot p \\ \gamma_q \cdot q \\ \gamma_r \cdot r \end{bmatrix} \times (P_R - O) \tag{24}$$

where the array of γ_*, with subscripted each linear and angular velocity, is a set of parameters which accounts for eventual flow deceleration and straightening in the fashion of MMG modelling.

Then, the local velocities are rotated into the fin mounted reference frame according to angle of installation Γ (see Fig. 5), with: c_0 aligned with the chord , t_0 perpendicular to the thickness of the fin, and s_0 along the span pointing outward – see Fig. 6. The rotation in between the *local-reference* to the *rudder-reference* is:

$$\begin{bmatrix} t_o \\ c_o \\ s_o \end{bmatrix} = R_{(\Gamma)} \begin{bmatrix} u_R \\ v_R \\ w_R \end{bmatrix} \qquad R_{(\Gamma)} = \begin{bmatrix} 1 & 0 & 0 \\ 0 & \cos\Gamma & \sin\Gamma \\ 0 & -\sin\Gamma & \cos\Gamma \end{bmatrix} \tag{25}$$

Once the fin mounted reference is set, the methodology identifies the parallel and perpendicular directions of the inflow, thus determining the lift and drag action lines – rotated of β_R along s_o. Specifically: the local drift angle β_R is calculated as follows:

$$\beta_R = \tan^{-1}\left(\frac{t_o}{c_o}\right), \quad V_R = \sqrt{t_o^2 + c_o^2} \tag{26}$$

And the rotation matrix in between the *rudder-reference* and the *inflow-reference* is:

$$R_\beta = \begin{bmatrix} \cos\beta_R & \sin\beta_R & 0 \\ -\sin\beta_R & \cos\beta_R & 0 \\ 0 & 0 & 1 \end{bmatrix} \tag{27}$$

Finally, the effective angle of attack is evaluated as the difference between the geometric angle and the in-flow angle of attack as stated in Eqs. (16) for the movable part, and (17) for the fixed part.

This enables the assessment of lift L and drag D (see the force vectors in red – Fig. 6) for the control plane generically installed in space. The lift and drag forces are then evaluated based onto Eqs. (18) and (19) as follows:

$$L = C_L(\delta_{Re}, \alpha_{fe}) \cdot \frac{1}{2}\rho A(\delta_{e_R}) \cdot V_R^2, \quad D = C_D(\delta_{Re}, \alpha_{fe}) \cdot \frac{1}{2}\rho \cdot A(\delta_{e_R}) \cdot V_R^2, \quad S = 0 \tag{28}$$

Finally, the forces in the *inflow-reference* are reported back to *submarine-reference*, by reversing the order of the rotations, as in the following:

$$\begin{bmatrix} X_R \\ Y_R \\ Z_R \end{bmatrix} = R_\Gamma^T R_\beta \begin{bmatrix} -D \\ L \\ S \end{bmatrix} \tag{29}$$

$$\begin{bmatrix} K_R \\ M_R \\ N_R \end{bmatrix} = \begin{bmatrix} x_R \\ y_R \\ z_R \end{bmatrix} \times \begin{bmatrix} X \\ Y \\ Z \end{bmatrix} \tag{30}$$

The calculation is updated at each time step and summed to the other force and moment contributions. The procedure is applied for each fixed and movable appendage.

4.7. Out of planes forces

The interactions between the sail and the bare hull significantly influence submarine manoeuvrability.

When straight sailing, the presence of the sail introduces an asymmetry of the pressure field onto the hull in the vertical direction, which generates a downward vertical force downstream the sail wake and a nose-up pitch moment. Stern control surfaces are endorsed of neutralising these effects, thus maintaining a stable trim and constant depth.

Moreover, during horizontal-plane manoeuvres (e.g., turning circle or zig-zag), the sail is subjected to hydrodynamic lift. The pressure differential across its two sides generates a vortex that detaches from the tip and propagates downstream along the upper surface of the hull. This

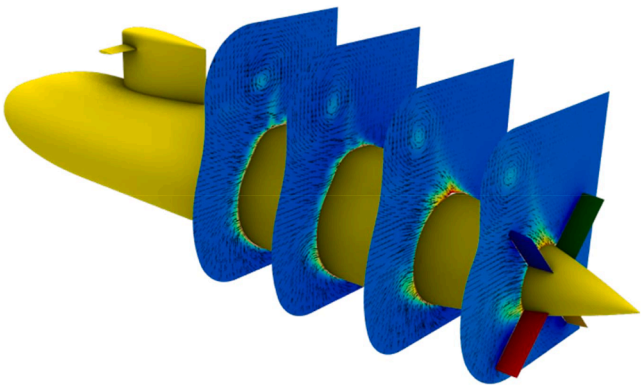

Fig. 12. BB2-Pure Drift: Tip vortex shed from the sail.

generates a tangential velocity near the upper hull surface opposite to the local drift component, thereby reducing the average cross-velocity. Globally, the tip-vortex produces a cross-flow blockage on the upper hull surface, while the lower surface experiences a cross-flow acceleration. Consequently, a high-pressure region develops on the upper side and a low-pressure region forms beneath. This pressure distribution produces a downward vertical force acting on the aft portion of the hull downstream of the sail. The resulting force system induces a positive pitch moment and causes a depth variation commonly referred to in the literature as *stern dipping*.

As an example, Fig. 12 shows a simulation of pure drift in the horizontal plane, with a drift angle of $\beta_H = 10°$. The vortex generated by the sail and its propagation towards the stern are clearly visible.

4.7.1. Model - pure drift

The DITEN semi-empirical proposed model starts from the SUB+ and calibrated on SUBx and BB2 submarines, by analysing the hull and sail geometries and their repartition of forces in terms of PMM tests - without control planes contribution. In particular, by analyzing the horizontal pure drift motion, the vertical Z force is seen to be satisfactorily

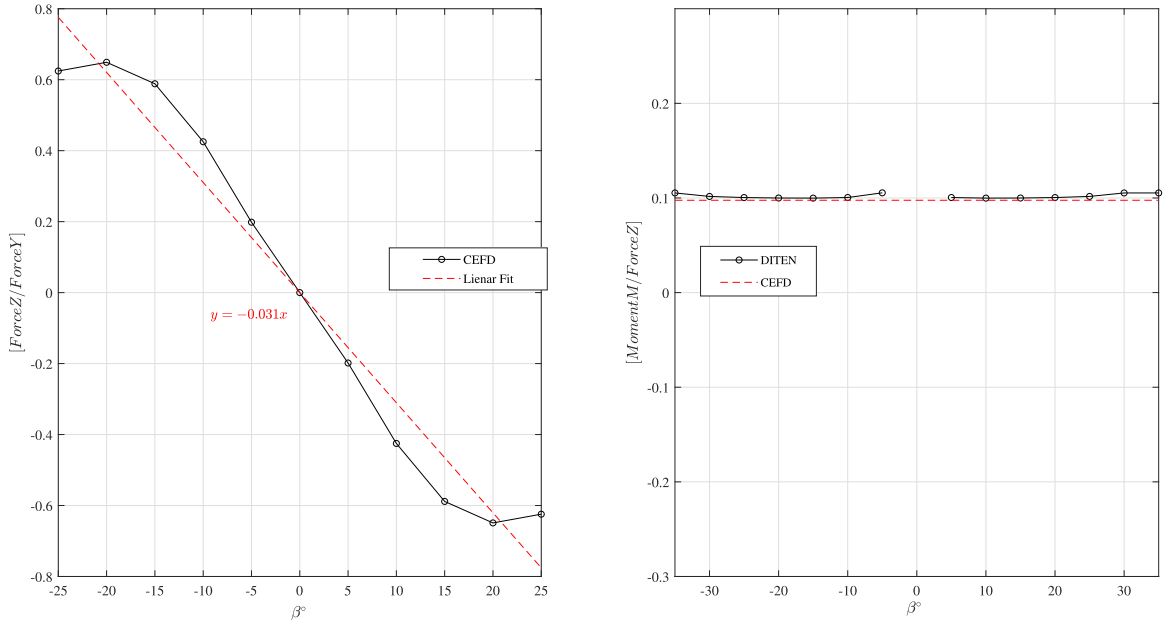

Fig. 13. Correlation out/in plane forces - SUB+ experiments.

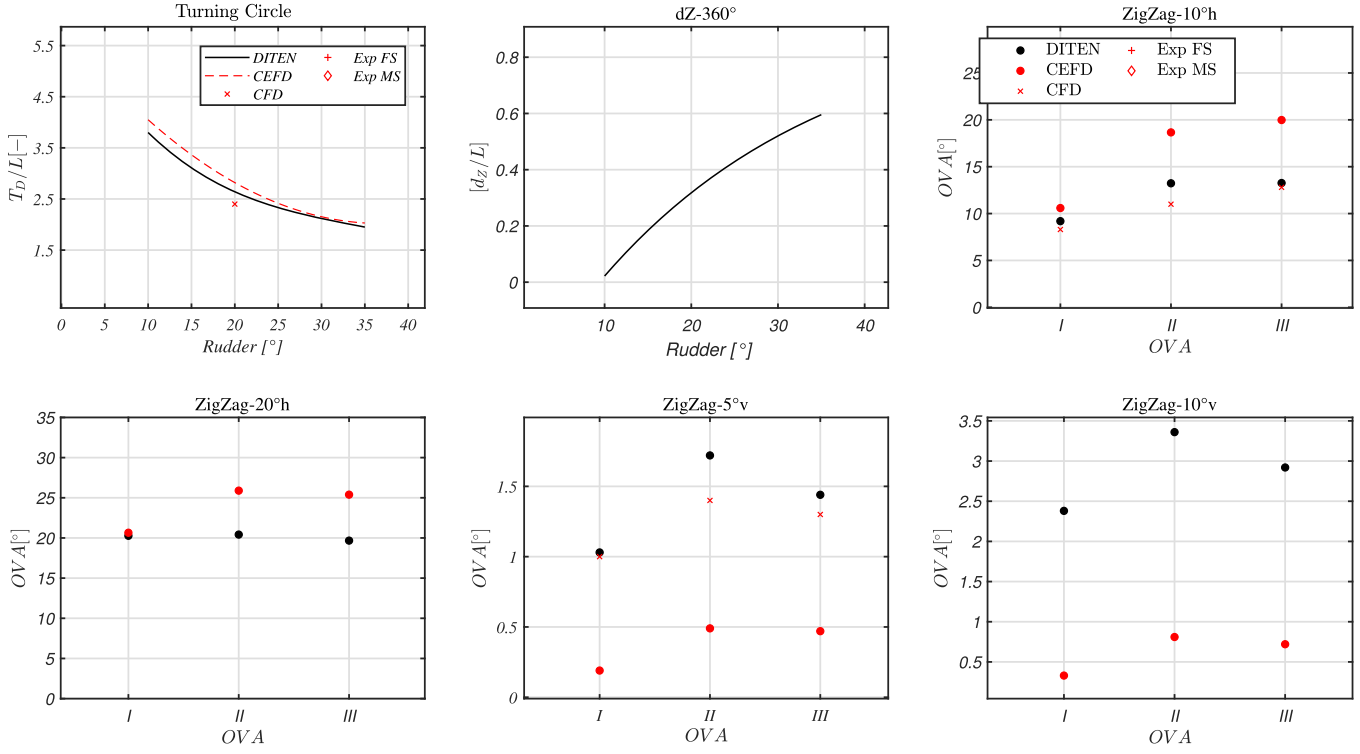

Fig. 14. SWE manoeuvres results.

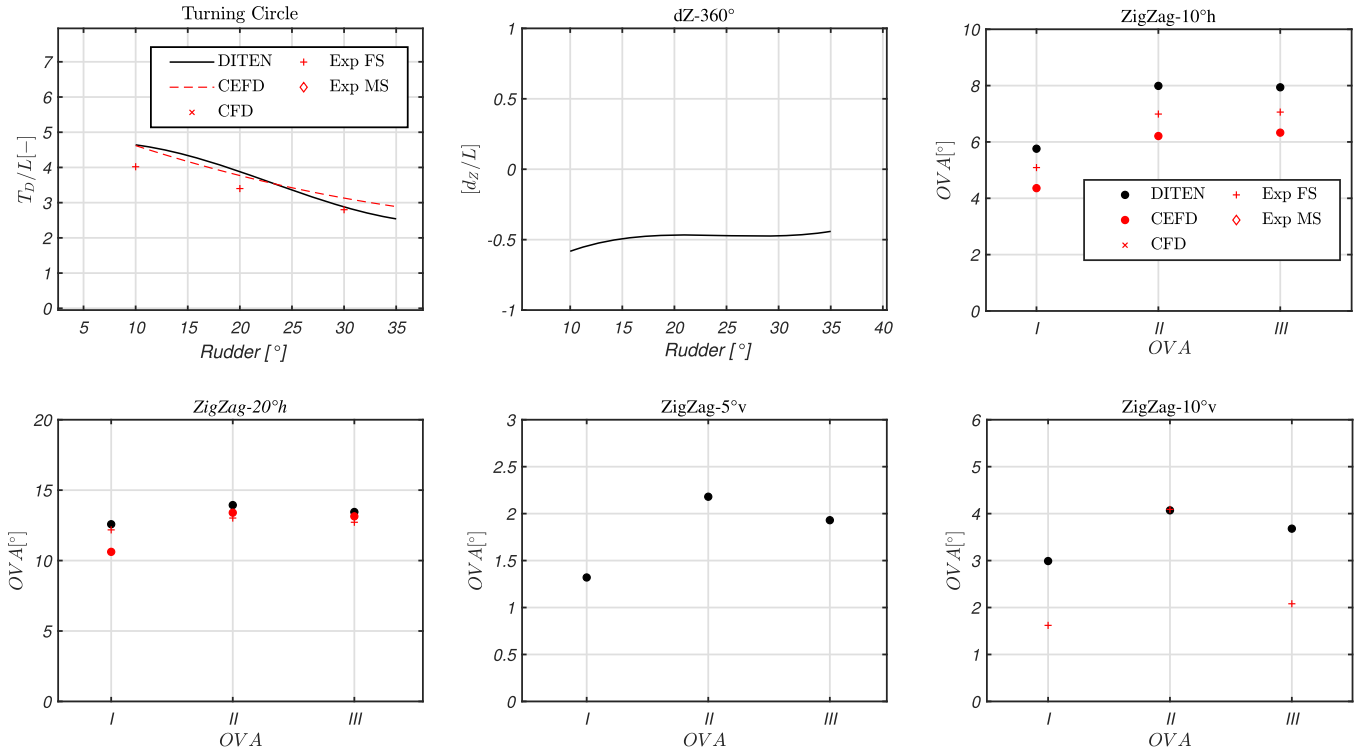

Fig. 15. BB2 manoeuvres results.

proportional to the horizontal Y drift force of *hull+sail* (subscript HS), according to the following Figs. 13 – left side . In terms of equations, the vertical hull due to the sail becomes:

$$Z_H^S(\beta_H) = -(0.031\beta_H)Y_{HS}(\beta_H) \cdot k_{vtx} \tag{31}$$

where k_{vtx} is a reduction factor according to Feldman theory (Feldman, 1979), which accounts for the detachment of the vortex from the hull after the threshold value $\hat{\beta}_H = atan(\ell_{vtx}/0.5B)$, with ℓ_{vtx} the length of the path traced from the vortex along the hull, according to the following equation:

$$k_{vtx}(\beta_H) = \begin{cases} 1, & \text{if} \quad \beta_H \le \hat{\beta}_H \\ 1 - \dfrac{\beta_H - \hat{\beta}_H}{\tilde{\beta}_H - \hat{\beta}_H}, & \text{if} \quad \hat{\beta}_H < \beta_H \le \tilde{\beta}_H \\ 0, & \text{if} \quad \beta_H > \tilde{\beta}_H \end{cases} \tag{32}$$

In this simplified method, the vortex path is considered to follow a potential streamline according to the angle of drift β_H; the transition of the detachment of the vortex from the hull starts at $\hat{\beta}_H$ and completes at $\tilde{\beta}_H = 40°$ – based on Feldman (1995) and DITEN available data.

On Fig. 26, the agreement of the DITEN model against the PMM can be satisfactoirily verified in terms of Z force.

In addition, the pitching moment M is found to be proportional to a constant value, which physically can be interpreted as the arm of the Z force - i.e. the point of application x_{vtx} – see Fig. 13 – right side. This arm can be found according to the length of the path ℓ_{vtx} traced from the vortex along the hull, starting from the coordinate of the trailing edge of the sail x_s^{TE}:

$$x_{vtx}(\beta_H) = x_s^{TE} - 0.25\ell_{vtx} \quad M_H^S(\beta_H) = -x_{vtx} Z_H^S(\beta_H) \tag{33}$$

In the Section 5.3, the agreement of the DITEN model against the PMM it is verified in terms of M moment.

4.7.2. Model - sail geometry dependence

Starting from the previous formulation for one single geometry, the DITEN model includes a generalization for different types of submarine sail+hull geometries, based onto four principles:

- Proportionality of Z force based onto total hull + sail Y^{h+s} force based - see Eq. (31)
- Dependency of Z force based onto vortex detachment at drift - see Eq. (32)
- Dependency of M moment onto sail-vortex shed path ℓ_{vtx} and pressure field arm - see Eq. (33)
- a linear regression based onto the ratio of linear lateral forces generated by the hull Y_v^H and sail Y_v^S separately exposed to h-drift, has been included, according to the following:

$$K_{Y_v} = \frac{Y_v^S}{Y_v^H} \quad \tilde{K} = (1 + (K_{Y_v}/K_{Y_v}^{STD} - 1)) \tag{34}$$

where $K_{Y_v}^{STD}$ is the reference evaluated SUB+ coefficient. It can be observed, that in case of absence of sail, $K_{Y_v} = 0$, i.e. the stern dipping force becomes zero.

4.7.3. Model - drift and yaw

Differently from literature (Kim et al., 2023), which separately include pure drift, pure yaw and drift+yaw stern-dipping terms, the DITEN model unites the effects explicitly according to the sail local angle of attack δ_{Se} according to the following:

$$\delta_{Se} = -\beta_H^s \quad \beta_H^s = atan(v + rx_s/u) \tag{35}$$

In particular, since the sail is installed forward mid-submarine, the crossflow components tend do cancel out - i.e. v and rx_s are opposite in sign. The reduction itself of the angle of attack leads to a reduction of vortex intensity, and as a consequence, this is deemed to be responsible of the reduction of the stern dipping force and moment. The above equations dependencies thus are modified according to β_H^s.

As a conclusion, the final equations become:

$$Z_H^S(\beta_H, r) = Z_H^S(\beta_H^S) \cdot \tilde{K} \quad M_H^S(\beta_H, r) = -x_{vtx} \cdot Z_H^S(\beta_H, r) \tag{36}$$

5. Results

The study presents results in four subsections. The first Subsection 5.1 reviews the primary manoeuvring parameters

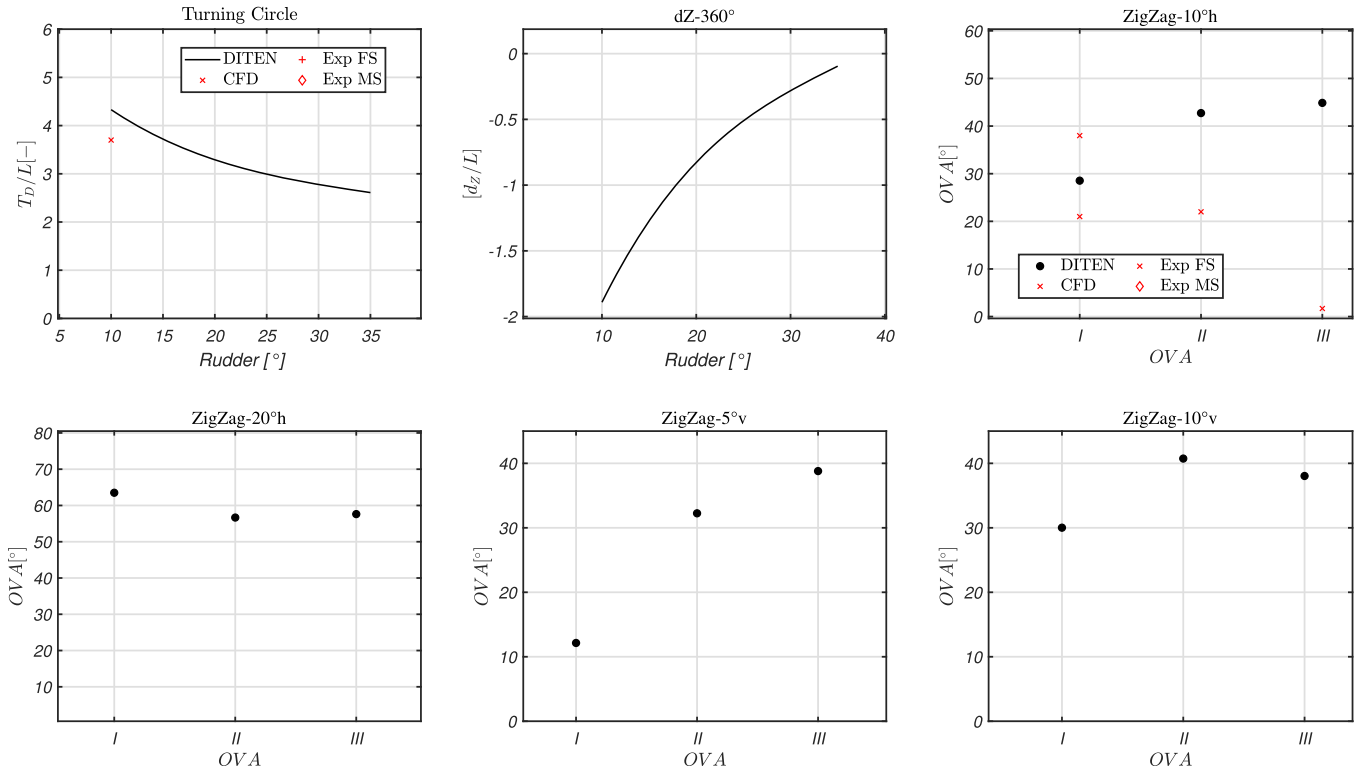

Fig. 16. SUBOFF manoeuvres results.

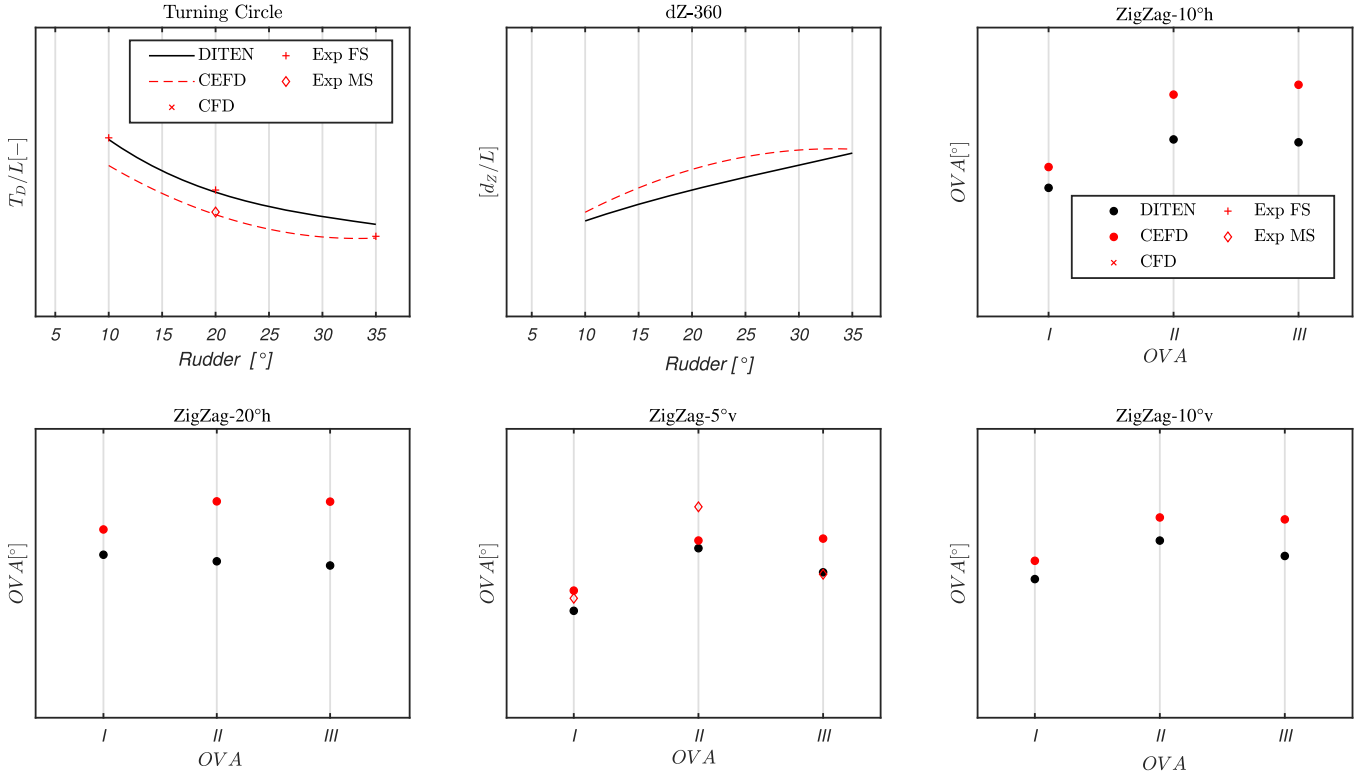

Fig. 17. SUB+ manoeuvres results, y-axis omitted.

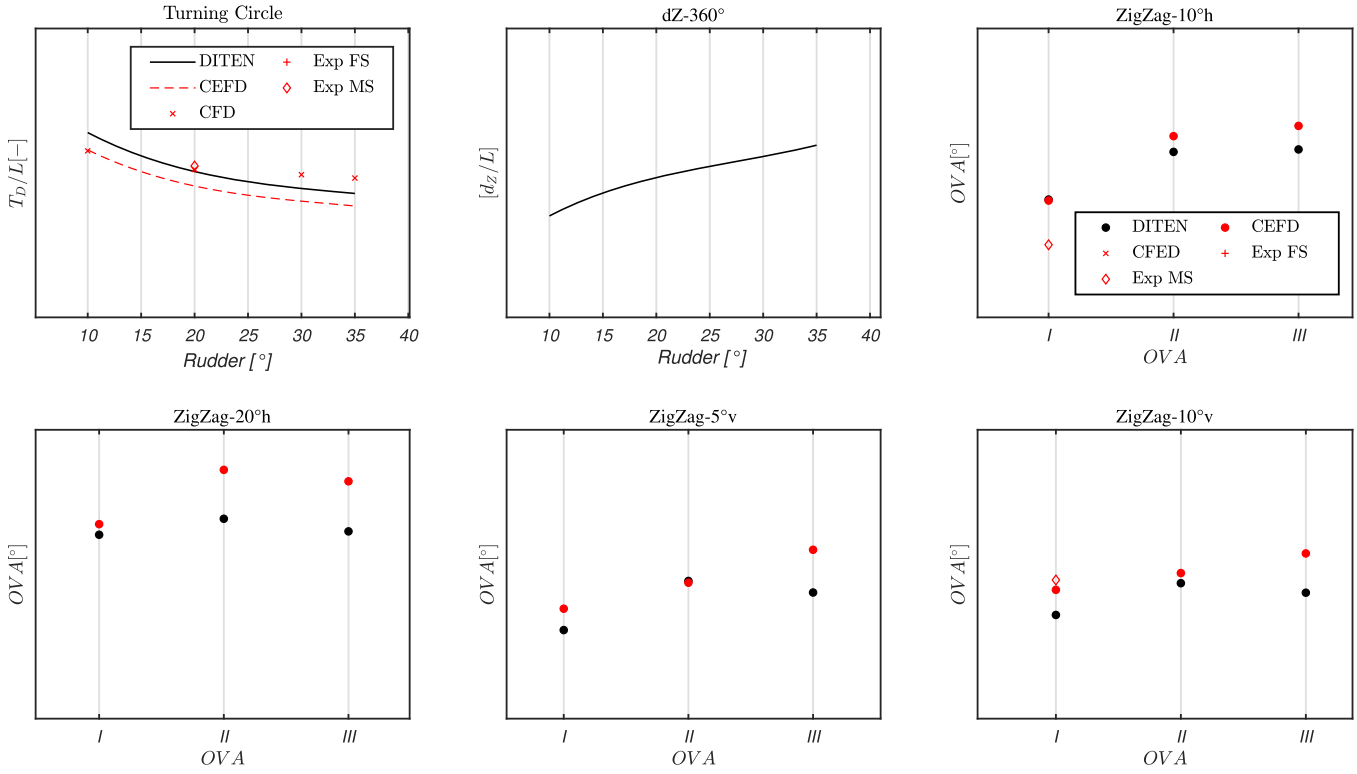

Fig. 18. SUBX manoeuvres results, y-axis omitted.

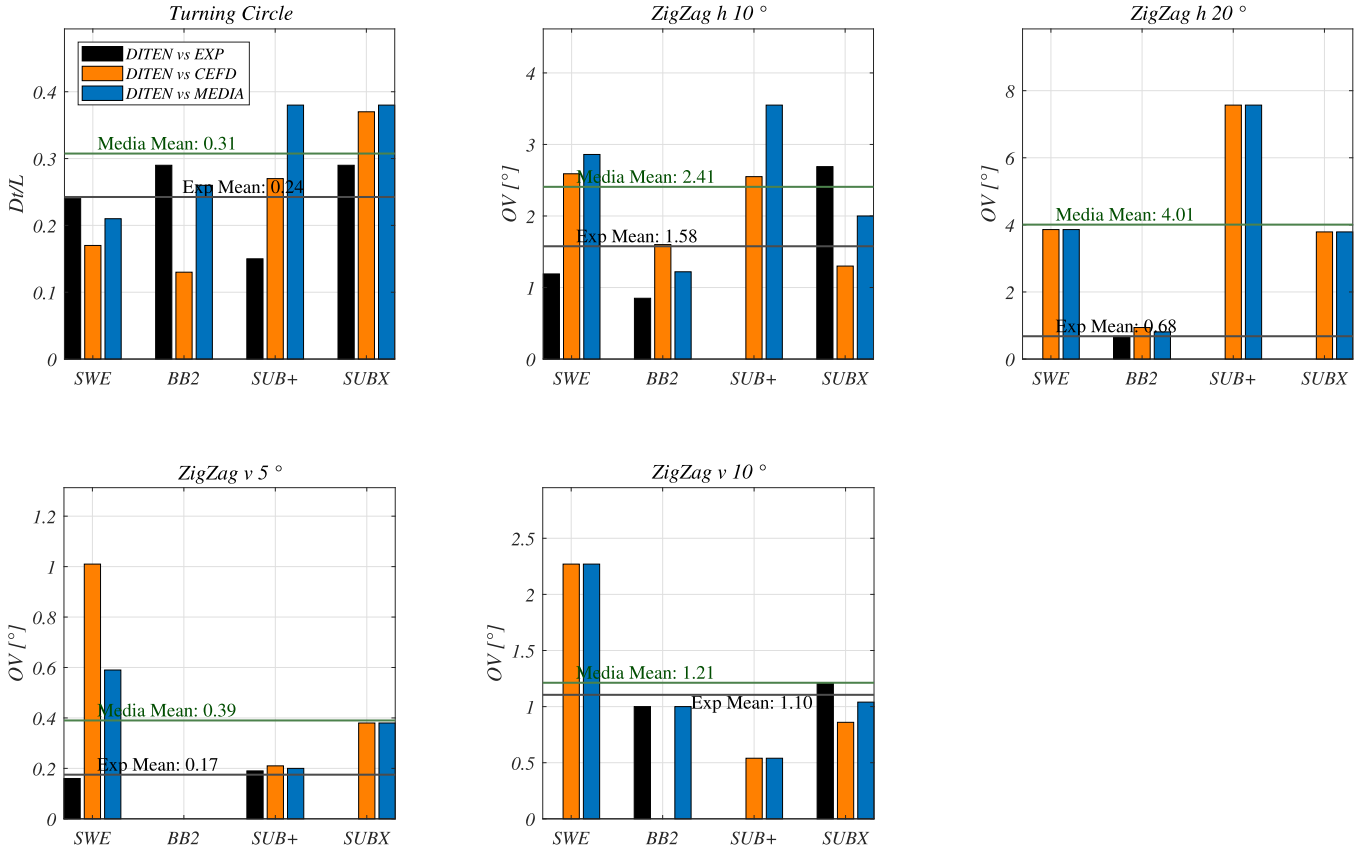

Fig. 19. Errors manoeuvres.

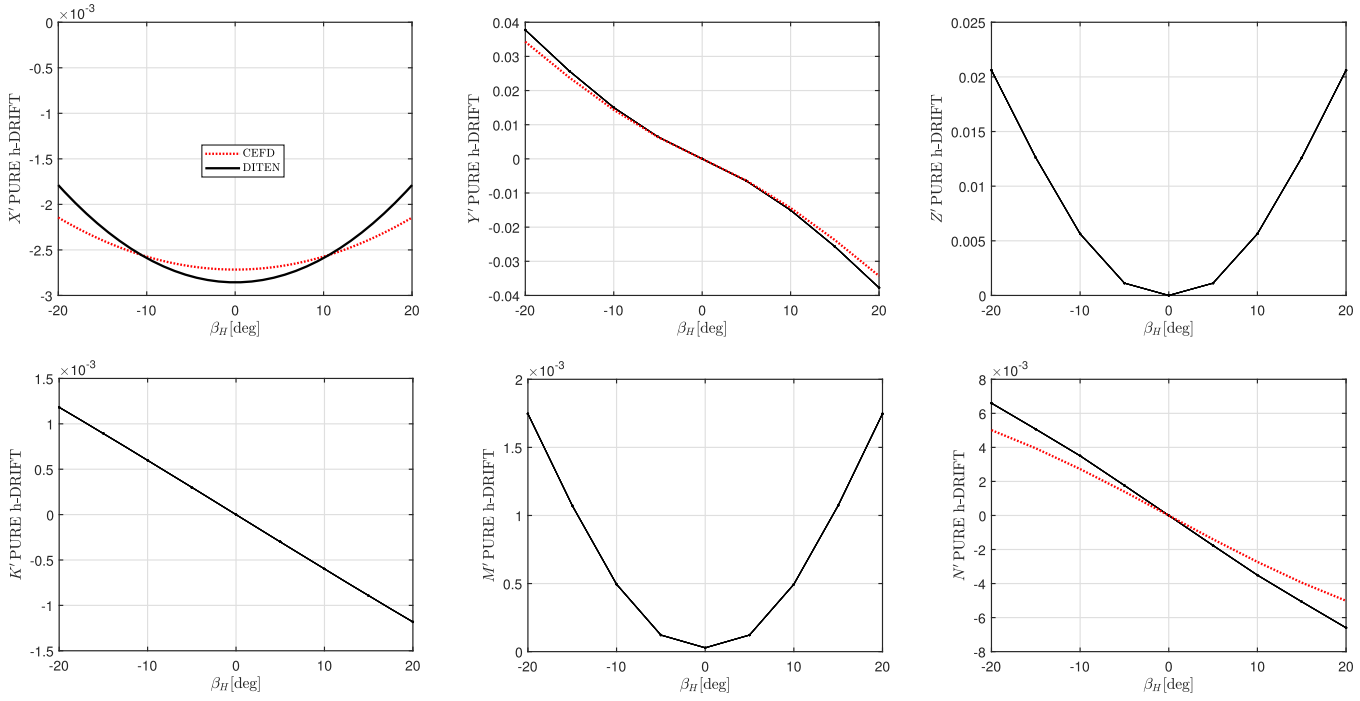

Fig. 20. BB2 pure horizontal drift.

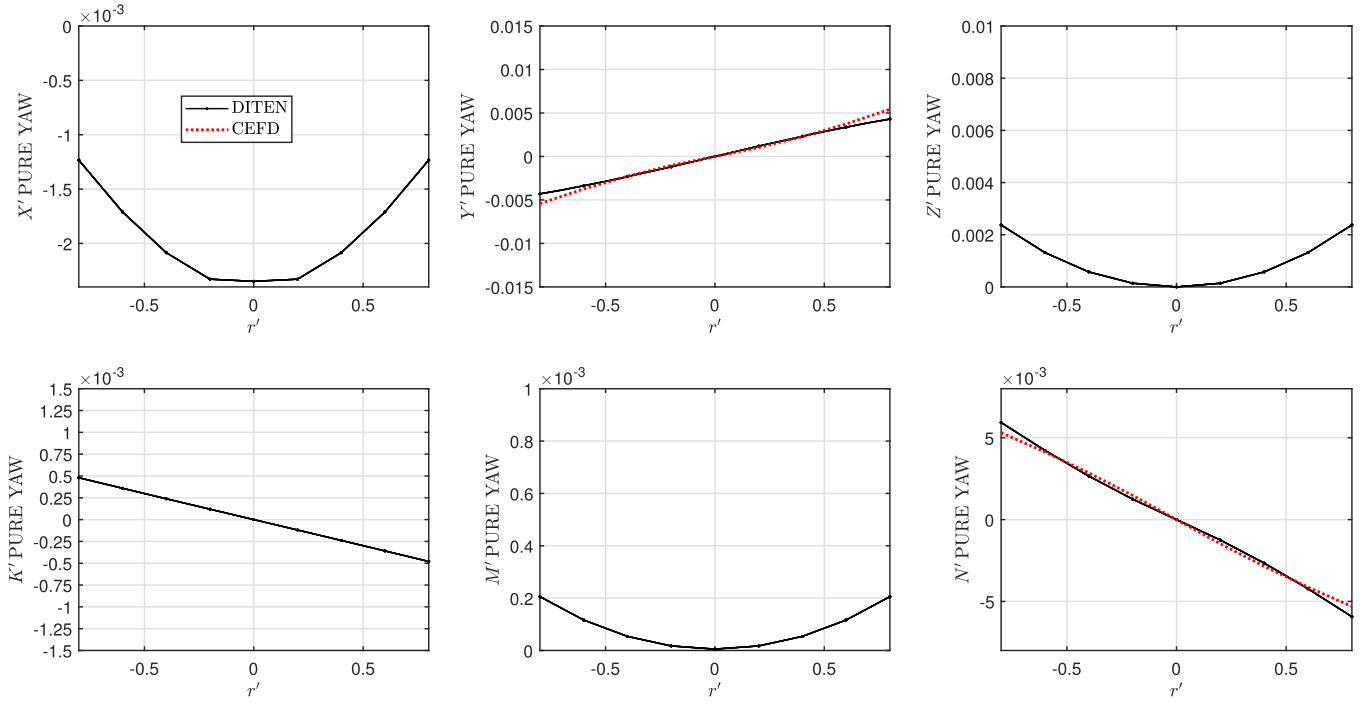

Fig. 21. BB2 pure yaw.

simulated with DITEN and compares them with available reference data, considering separately the different vessels of the case study. The second Subsection 5.2 quantifies the global mean error of the DITEN model against the whole test case, allowing to have an insight into the expected overall discrepancies.

Then two further analyses are present, in order to get a more direct insight of some issues. In particular, the third Subsection 5.3 analyses the simulated PMM for the BB2 and SUB+ vessels using the CEFD and DITEN models. As it will be seen, due to data confidentiality, the PMM graphs for the SUB+ vessel exclude axis labels, not precluding a general overview of the results. The last Subsection 5.4 examines the time histories of key parameters for three manoeuvres: a 20° turning circle, a Zig-Zag 10° in the horizontal plane, and a Zig-Zag 5° in the vertical plane for the BB2 vessel. The graphs provide a direct comparison between the DITEN and CEFD models, allowing to have a further insight into the problem and highlighting further areas of improvement.

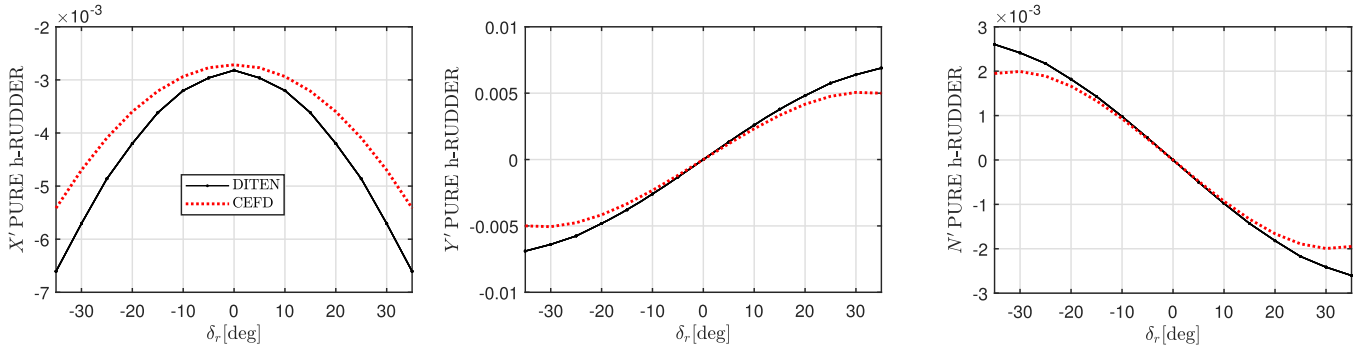

Fig. 22. BB2 pure horizontal rudders.

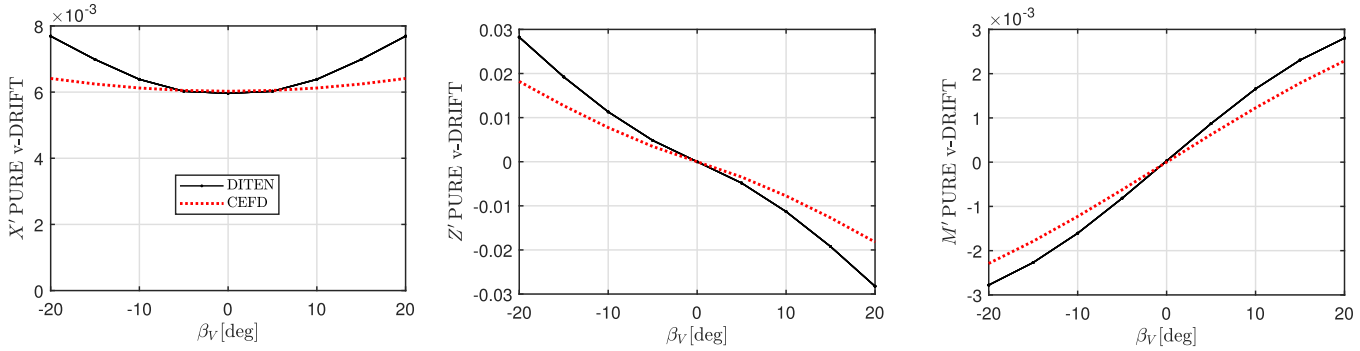

Fig. 23. BB2 pure vertical drift.

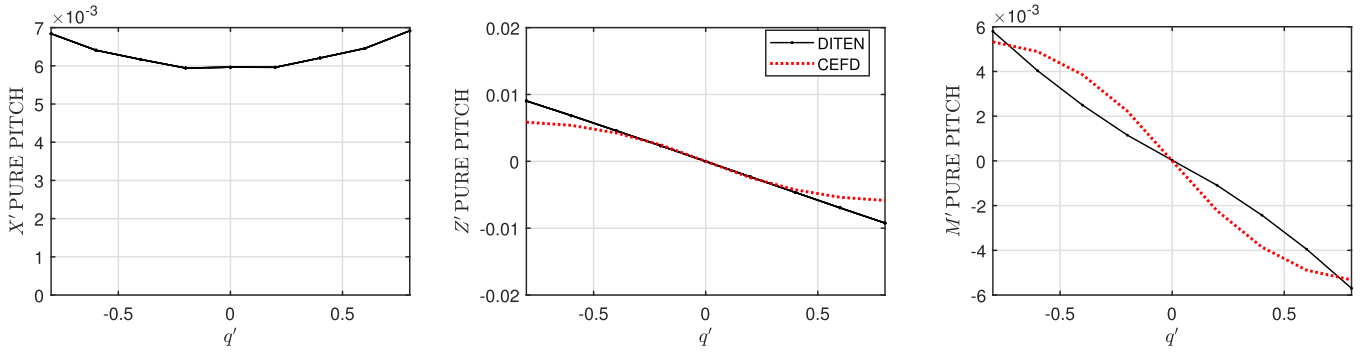

Fig. 24. BB2 pure pitch.

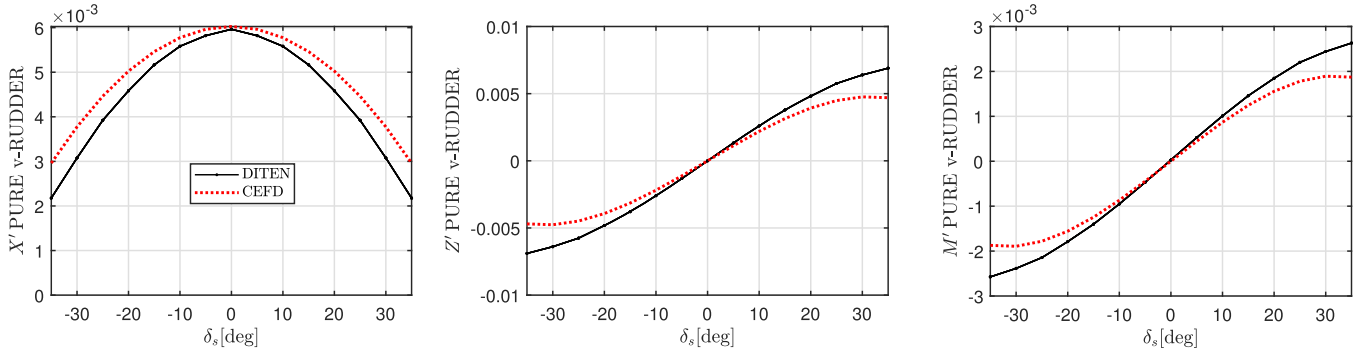

Fig. 25. BB2 pure vertical rudder.

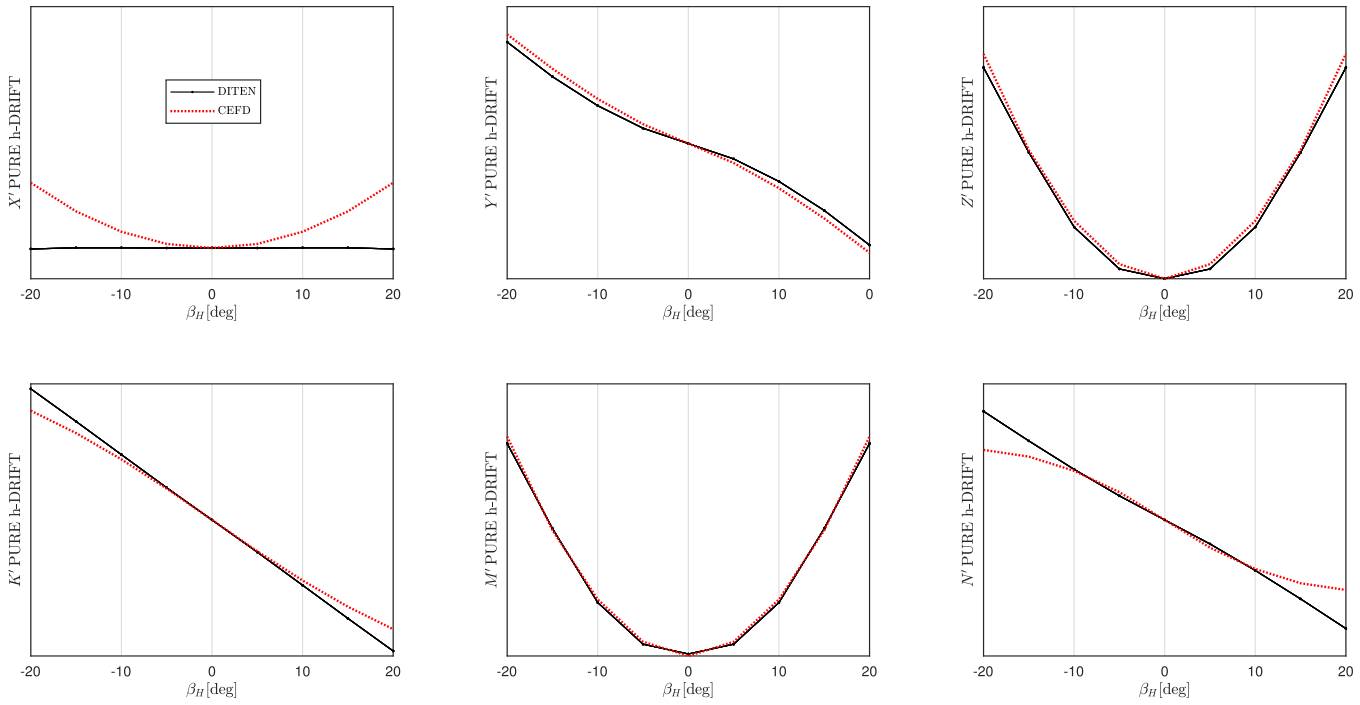

Fig. 26. SUB+ pure horizontal drift.

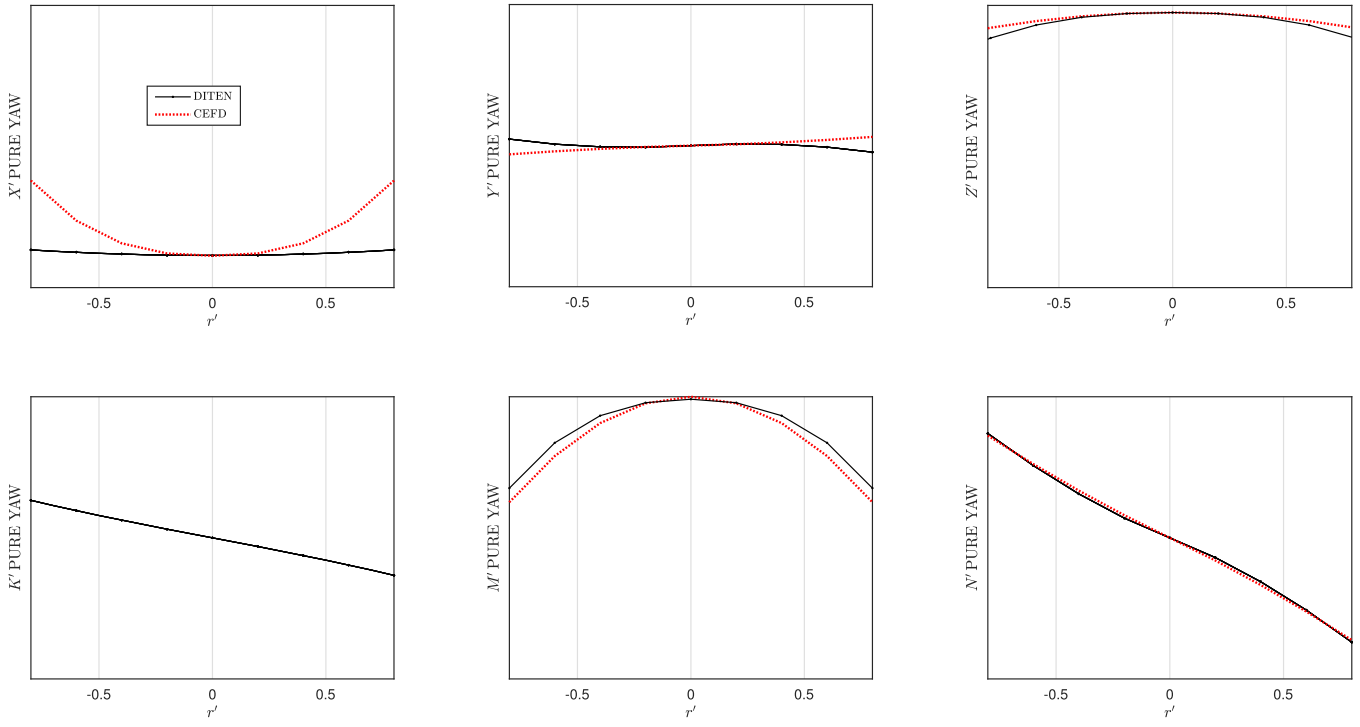

Fig. 27. SUB+ pure yaw.

5.1. Comparison of global manoeuvring parameters.

The following section presents the results of the DITEN manoeuvring prediction simulations carried out on the case study vessels.

The following manoeuvres have been simulated:

- The Turning Circle (TC) manoeuvre characterizes the vessel's ability to complete a turning trajectory (turning ability) in response to a fixed rudder angle. Starting from initial forward motion only, a constant helm angle is applied and the vessel is allowed to evolve freely.
- The Zig-Zag (ZZ) manoeuvre is designed to assess the vessel's ability to change heading/depth in response to a moderate rudder angle (initial turning), and subsequently to neutralise this change in order to restore only forward motion (yaw checking). The manoeuvre consists of applying a rudder angle (10° or 20° in the horizontal plane, and 5° or 10° in the vertical plane), followed by a counter-rudder action upon reaching a target heading deviation of equal

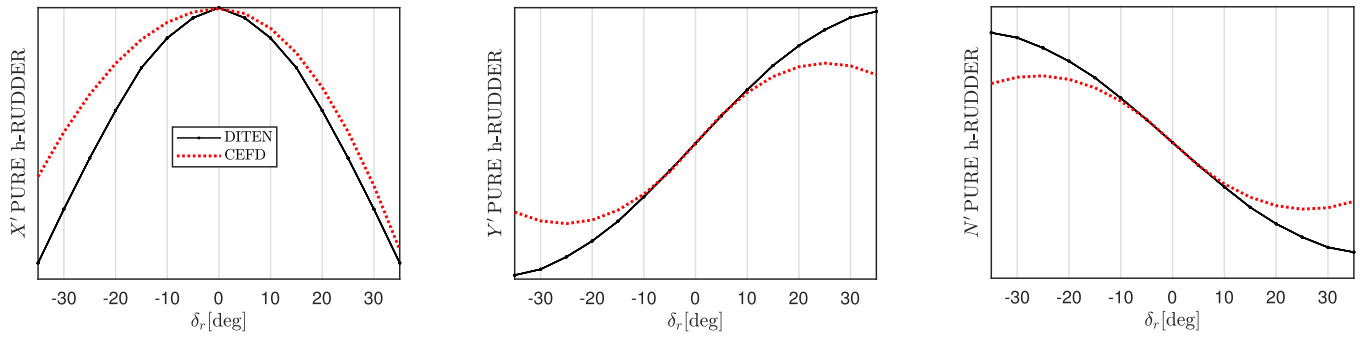

Fig. 28. SUB+ pure horizontal rudder.

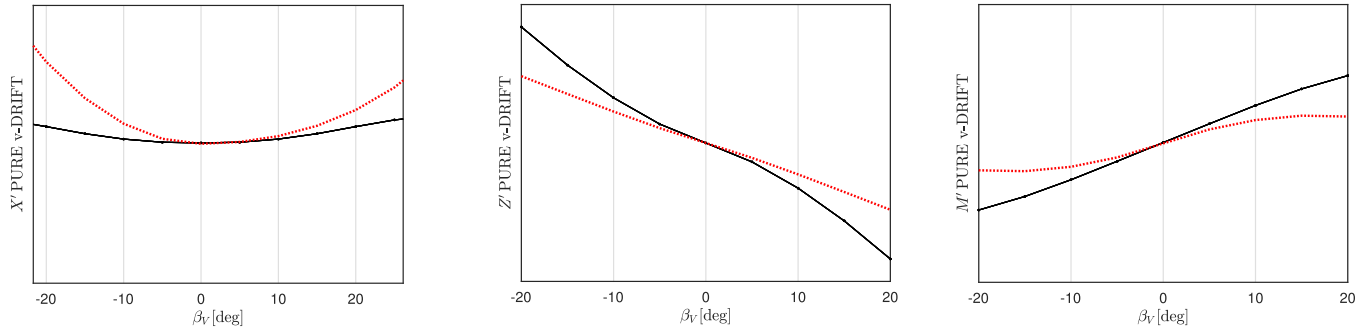

Fig. 29. SUB+ pure vertical drift.

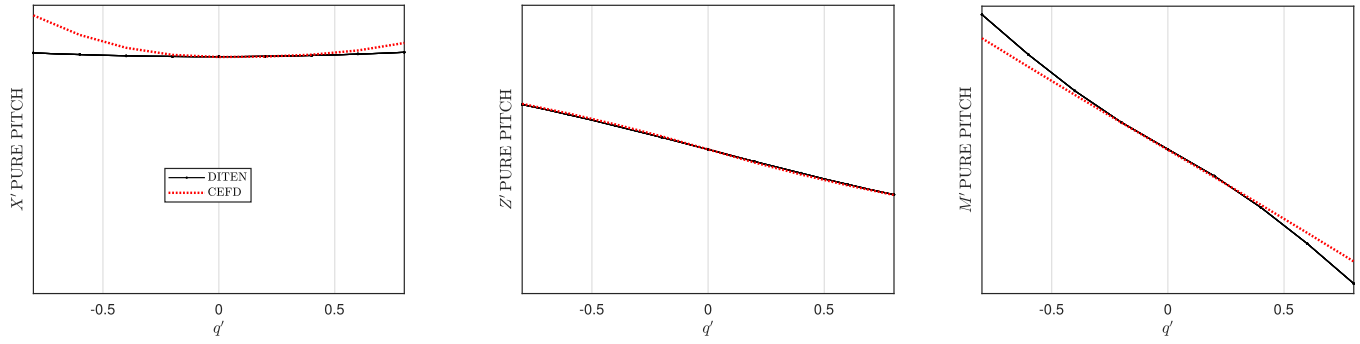

Fig. 30. SUB+ pure pitch.

magnitude. This is a cyclic manoeuvre, typically repeated for at least three consecutive rudder actions, and it is carried out in an analogous manner in both manoeuvring planes

It should be remembered that: for what regards horizontal manoeuvres, the TC is the most present in free running tests, thus allowing for a more direct and fair comparison; the horizontal zigZag manoeuvre is more problematic, with sparse data, sligthly more centred on ZigZag10h; the only data for the vertical 5° ZigZag manoeuvre relate to the SWE and SUB+ vessels derived from simulations; for the vertical 10° ZigZag manoeuvre, the only vessels with free running data available for comparison are BB2 and SUBX.

Moreover, it is important to remind, from this point of view, that complete CEFD models derived from PMM tests are available only for SUB+ and SUBx, while for the other cases only simulation results (and in some case with partial coefficients) are available, thus making the comparison less reliable. Data from CEFD (PMM) is available only for BB2, SUB+, and SUBX, while for the others data come from simulations.

In the following, results are presented, considering in particular the following parameters:

- The dimensionless tactical diameter **(TD/L)**.
- The overshoot angles **(OVA)** in horizontal zigzag manoeuvres, from the first to the third.
- The overshoot angles **(OVA)** in vertical zigzag manoeuvres,from the first to the third.
- The variation of depth quote during TC manoeuvres

In Figs. 14–18, the simulated results are reported for each submarine: in black bold line are presented the DITEN model results, while the red markers represent the reference experimental data (or data from the literature), and the red dashed curves correspond to the simulations conducted using experimental coefficients through the “CEFD” model – if available. For the SUB+ and SUBX vessels, the maneuvering characteristics are confidential data. Consequently, the presented graphs are without axis references.

As a first step, the results are discussed specifically for the five cases in the following:

- **SWE** – Fig. 14: The DITEN model captures the manoeuvring characteristics of the vessel with a good level of accuracy in both the

horizontal and vertical planes, closely matching the available experimental data. When analyzing the TC graph, the trend predicted by the DITEN model aligns perfectly with the only available experimental data point. Similarly, the curve produced by the CEFD model yields the same result. For ZigZag manoeuvres in the horizontal plane, the experimental values are well captured when present (10/10° ZigZag), while the CEFD model overestimates them. In the vertical plane for the ZZ05v manoeuvre, the DITEN model's curve precisely matches the available experimental data. The results from the CEFD model appear underestimating considerably the overshoots – a trend also observed in the ZZ10v manoeuvre. It appears in this case that the values of CEFD seem not very reliable. It has to be noted that the coefficients available in literature might be affected by errors, being part of a master thesis available in literature (Thuné, 2015).

- **BB2** – Fig. 15 experimental data are available for the BB2, particularly regarding zigzag manoeuvres, which are critical for verifying transient dynamics in terms of controllability. It is observed that the DITEN model accurately predicts both the trends and the values from experiments related to TC and ZZ manoeuvres in the horizontal plane (for both Zig-Zag 10 and Zig-Zag 20). In the vertical plane, a positive correlation is also observed for the vertical Zig-Zag 10 manoeuvre, although with overestimation of first and third overshoot. The CEFD model curve, which employs the coefficients outlined in the referenced publication (Joubert, 2004), exhibits a high degree of correlation with the experimental outcomes in the horizontal plane, thereby demonstrating robust predictive capabilities. The BB2 CEFD-based manoeuvres for the vertical plane have been excluded from the analysis due to an unexpected divergent behaviour.
- **SUBOFF** – Fig. 16: the vessel - well known for his inherent instability (as stated by the DTRC itself - see geometry with reduced rudders and almost no sail), lacks of accurate experimental comparison data. Only a few partial simulations are available from the existing literature. Therefore, any reference should be taken as an indication of general trends, considering also the great dispersion, where available. Nevertheless, the only available data in the TC were accurately identified. The observation of the overshoot behaviour demonstrates that the vessel's pronounced instability results in significant overshoots in the ZZ10h, which eventually diverge in the ZZ20h.
- **SUB** + – Fig. 17: For this vessel CEFD coefficients (in this case coming from PMM model tests) lead to a very good correspondence with free running tests, thus allowing to provide a fair comparison also for manoeuvres not available in free running configuration. For what regards manoeuvres in the horizontal plane, a very good correspondence is present for the turning circle manoeuvre, while for the ZigZag manoeuvre the overshoot angles are underestimated. The trend of depth variation during the turn is also accurately captured. Also vertical overshoot angles appear captured with sufficient accuracy, both in trend and in absolute values, with only a slight underestimation.
- **SUBX** – Fig. 18: In this case, experimental results are available mainly for TC manoeuvre, with only one result for horizontal ZigZag and one for the vertical ZigZag. CEFD results are available (with data from PMM), thus allowing to enlarge the comparison also to other manoeuvres. Turning circle results present a very good correspondence, while a tendency towards overestimation exists for overshoot angles in the horizontal manoeuvres. For what regards the vertical ZigZag manoeuvre, a tendency towards underestimation is observed.

5.2. Global errors

After the first analysis of the specific test cases, it is worth considering a more general analysis of the whole results, in order to assess the overall capability of the model to capture the manoeuvrability characteristics of the fleet submarines. In order to do this, the SUBOFF test case has been eliminated, since it presents a too large difference in terms of quality confidence with respect to the others. Moreover, in order to manage the vast dispersion of data available, its inherent quality, and to guarantee the reader a usable reading, it was decided to consider three main error values described below:

Table 3
Summary of average errors on all test case.

MAN	DITEN vs EXP	DITEN vs MEAN	MEAN DATA
TC	0.24	0.31	3.3
ZZh10	1.58°	2.41°	12
ZZh20	0.68°	4.01°	22
ZZv5	0.17°	0.39°	1.5
ZZv10	1.10°	1.21°	2.5

1. Errors of the DITEN model from the most reliable experimental data (where available) (namely: **DITEN VS EXP**), i.e. in order of priority:
   (a) full scale
   (b) model scale
   (c) simulations and literature
2. DITEN model error compared to simulated data with CEFD model (namely: **DITEN VS CEFD**)
3. DITEN model error with error obtained by averaging all experimental data with simulated CEFD model data (namely: **DITEN VS MEAN**)

In addition to this, in order to provide more easily understandable data, only the average error over the three turning circle tests conducted at different rudder angles (10°, 20°, 30°) have been considered.

Similarly, the average error among the three overshoot angles in both manoeuvring planes is considered for the Zig-Zag manoeuvers. In Fig. 19, the errors are reported with 'DITEN vs EXP' (plotted in black), 'DITEN vs CEFD' values (plotted in orange), and 'DITEN vs MEAN' values (plotted in blue). Additionally, each graph includes a horizontal line indicating the average error of the DITEN model, averaged over all vessels considered in this analysis: the number plotted in black represents the 'DITEN vs. EXP' comparison, while the number plotted in green corresponds to the 'DITEN vs. MEAN' comparison.

For a further summary, Table 3 reports all the mean values of the errors obtained, together with the mean value of the parameter considered, in order to have an idea about the average percentage error.

From the results, presented, it is clear that for turning circle manoeuvre, the average error settles around 0.3 L, thus globally a remarkably good correspondence, considering that the mean overall value of the TD for the different vessel is 3.3 L.

For what regards the horizontal zigzags, the errors are 1.58°/2.41° (EXP and MEAN) and 0.68°/4.01° for the ZigZag10° and ZigZag20° respectively. It has to be noticed that, for the ZigZag20°, only one experimental result is available, corresponding to the vessel for which the discrepancy is the least. In this case, therefore, the reference error to be considered is the MEAN one. Having this in mind, it is interesting to see that the average error is acceptable, being about 2° over a mean overshoot of 12° for the ZigZag10° and about 4° over a mean overshoot of 22° for ZigZag20°.

For what regards the zigzag manoeuvres in the vertical plane, the errors are 0.17°/0.39° (EXP and MEAN) and 1.21°/1.10° for the ZigZag5° and ZigZag10° respectvely. It has to be noticed that, in this case, for both manoeuvres the number of experimental data is limited, thus the reference error to be considered is the MEAN one. In this case it is clear that the relative error is larger, considering the mean of the parameters considered, highlighting the need for further analyses in future to improve its accuracy.

5.3. Hydrodynamic coefficients and PPM comparison

This subsection presents the PMM results for the BB2 (x-rudders) and SUB + (+-rudders) hulls. In the next figures, the black curve represents the PMM simulated using the DITEN model, while the red dashed curve

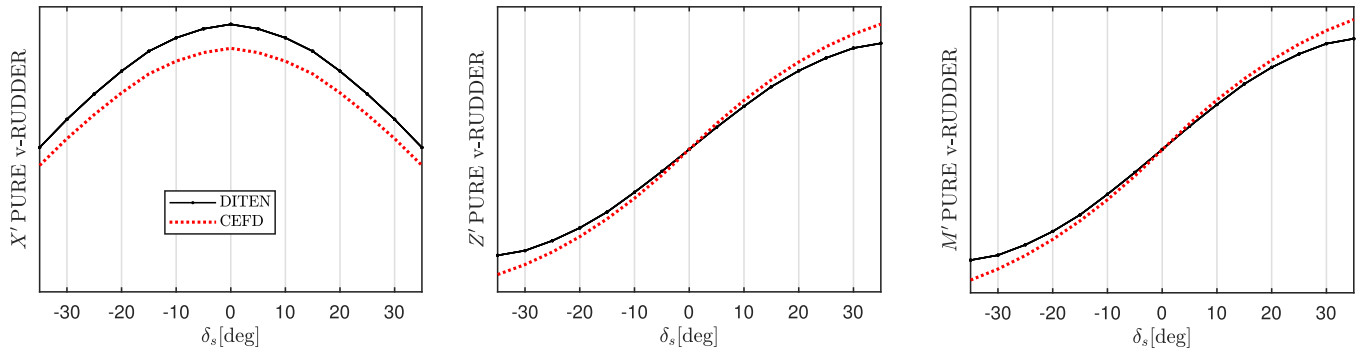

Fig. 31. SUB + pure vertical rudder.

corresponds to the PMM simulated with the CEFD set of hydrodynamic coefficients available for each submarine.

Figs. 20–25 depict the PMM results for the BB2 vessel. Overall, the DITEN model shows a sufficiently good accuracy in the horizontal plane. In Fig. 22, representing the pure horizontal rudders, a slight underestimation of the added resistance appears, along withan anticipated rudder stall in DITEN model. On the other hand, the vertical plane shows moderate disagreement between DITEN and CEFD results both in the case of pure pitch (see Fig. 24) and pure drift (see Fig. 23). In the pitch case, the second order forces result in a different curvature of the curve. The quality of the results for the pure vertical rudder, Fig. 25 is similar to those of the horizontal plane. It should be noted that the CEFD coefficients provided by the literature in the vertical plane were not validated through simulation, since they demonstrated a divergent behaviour; nevertheless, the corresponding PMM simulation is included in this study for comparison purposes. For actual comparison of the DITEN model, the experimental free-running test of the zz10v has been included in Section 5.4 (Fig. 35). The DITEN result underlines the fact that the model in the vertical plane may require additional modifications. Unfortunately, very limited data is available in literature for vertical motions, therefore this activity is left for future work, considering also that, globally, the behaviour of the vessel in the vertical plane is captured with sufficient accuracy, as shown by the following global result.

Figs. 26–28 show the PMM results for the SUB + vessel in the horizontal plane. The DITEN model shows again a sufficiently good agreement with the CEFD data. Looking at the horizontal drift (Fig. 26), the

Table 4
Hydrodynamic derivatives for literature vessels.

Coeff.	SWE		DARPA		BB2	
	DITEN	CEFD	DITEN	CEFD	DITEN	CEFD
X_v	−14.6041	24.2574	−4.9899	–	226.6023	232.7042
X_{vv}	12.6205	−10.4643	3.1358	–	−268.3544	−265.7131
X_w	92.1539	85.5336	64.9162	–	65.4642	60.4161
X_{ww}	−150.0687	−137.3858	−106.0964	–	−101.1505	−99.0145
Y_v	−47.8983	−64.3731	−34.2508	−29.149	−64.0379	−65.6832
Y_{vv}	−136.2234	−96.3851	−94.221	–	−130.354	−98.0202
Y_r	0.6094	−0.8241	3.3538	10.64	6.4641	4.601
Y_{rr}	−4.7536	−1.131	−1.5914	–	−1.6094	−2.715
Y_{δ_r}	18.3405	6.8806	9.4909	2.97	16.1595	15.1296
$Y_{\delta_r\delta_r}$	−9.9697	–	−4.0505	–	−14.426	−10.4446
Z_w	−22.8705	−24.9674	−21.3978	−14.57	−41.8407	−36.2556
Z_{ww}	−71.1719	−32.8881	−97.839	–	−75.9943	−47.9713
Z_q	−8.5591	−4.0505	−6.4772	−7.61	−13.0804	−13.95
Z_{qq}	1.5571	0.714	0.7488	–	0.6362	–
Z_{δ_s}	18.3405	7.2053	9.4909	5.60	16.1595	14.2725
$Z_{\delta_s\delta_s}$	−9.9697	–	−4.0505	–	−7.426	−9.8931
Z_v	3.6196	–	0.7927	–	3.7693	–
Z_{vv}	133.6806	–	83.0278	–	154.9813	–
Z_r	0.5473	–	0.022	–	0.06	–
Z_{rr}	−8.78	–	2.6464	–	3.78	–
K_v	−0.1178	−3.764	−0.0232	−0.61	−0.0903	–
K_{vv}	−1.1048	−5.9967	0.1465	–	0.2552	–
N_r	−5.7111	−4.5719	−3.7485	−4.43	−5.9658	−7.645
N_{rr}	−2.1002	−1.3509	−1.0508	–	−1.7258	−1.262
N_{δ_r}	−7.6983	−2.9395	−3.8413	−2.23	−6.1001	−6.0898
$N_{\delta_r\delta_r}$	4.1847	–	1.6394	–	4.8033	4.3583
N_v	−20.1969	−21.0953	−13.5498	−14.15	−20.6164	−17.0491
N_{vv}	−3.6224	−9.8946	1.7814	–	5.6595	7.7569
M_w	5.3316	5.2111	10.7929	10.74	8.9084	7.5611
M_{ww}	−2.5078	−2.8331	−6.4028	–	−5.0401	−2.8808
M_q	−3.6175	−3.0505	−2.403	−3.69	−14.8144	−12.62
M_{qq}	−1.9585	−1.1247	−2.0379	–	−12.5715	−7.456
M_{δ_s}	7.9521	3.517	3.8412	2.45	6.1584	5.6466
$M_{\delta_s\delta_s}$	−4.5958	–	−1.6393	–	−2.8978	−3.879
M_v	0.3969	–	0.0098	–	0.3348	–
M_{vv}	5.6256	–	2.3238	–	12.9812	–
M_r	0.23	–	0	–	0.026	–
M_{rr}	0.7455	–	0.2	–	0.72	–

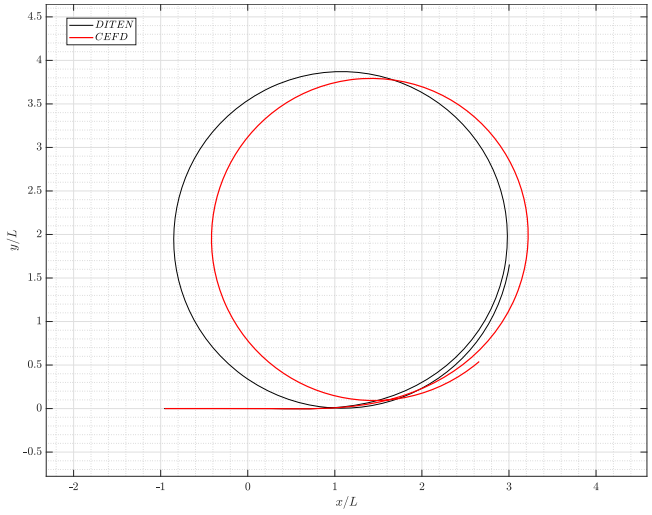

Fig. 32. BB2: turning circle 20° - trajectory.

N moment at large values of drift appears underestimated, while a large discrepancy appears for the X force; the out-of-plane forces appear very well captured. In Fig. 27, which refers to the pure yaw, a discrepancy in drag prediction is visible; unfortunately, the CEFD data for roll moment K are not available. The Y force overall matches the CEFD trend in the linear range, while it slightly loses quality outside this range. Fig. 28 highlights the same issue in capturing the rudder stall observed in the BB2 case. Figs. 29–31 show the results in the vertical plane. The DITEN model overestimates force and moment in pure vertical drift, even if in this case to a larger extent. On the contrary, discrepancies for pure pitch are reduced with respect to BB2 case. The pure pitch force and moments are well captured. The rudder forces seems in this case well predicted, also in terms of nonlinear effects.

To summarize the PMM results, Table 4 reports the first- and second-order pure hydrodynamic coefficients for SWE, SUBOFF, and BB2, extracted from the respective models, by means of regression – where available. As it can be seen, the linear coefficients (and the trends of the others) are in line with expectations and to the previously shown results, even if it is always difficult to comment on numerical values of sets of coefficients.

In general, this analysis shows that the model built allows to get a general qualitative agreement with available data, with better results in horizontal plane (where the discrepancies are rather limited, apart for the Y force of the SUB+) than in the vertical plane, which needs further studies in future, as already anticipated in the more general analysis reported in previous paragraphs. The rudder force is captured sufficiently well, with however a tendency towards underestimation of stalling phenomena, which is worth being further investigated, also in terms of the effect on the manoeuvres. From this point of view, considering that the effective rudder angle is normally reduced with respect to the geometrical one, it is expected that the effect should be rather limited, but certainly present.

5.4. Time histories comparison

This section compares the time histories of three manoeuvres for the BB2 vessel. The manoeuvres presented are a 20° Turning Circle, a horizontal ZigZag 10°/10°, and a vertical ZigZag 10°/10°. The results simulated with the DITEN model are shown in black, while the results simulated with CEFD are shown in red. Figs. 32 and 33 presents the results for the Turning Circle, while Figs. 34 and 35 show the results for the ZigZags. In the vertical plane, the free running model testing results have been included as a reference, since the CEFD model unexpectedly did not provide consistent values; it is important to mention that the quality of the CEFD vertical coefficients remains unverified. Moreover, the CEFD roll and stern dipping coefficients are not available for BB2 vessel – thus the curves are not shown in any of the next figures.

Observing Figs. 32 and 33, which present the main manoeuvre characteristics of the Turning Circle 20°, a good prediction by the DITEN model is observed compared to the simulated CEFD, comprehensively of the transient stages. In terms of trajectories, a good overlap between the time histories of the two prediction models is also noted and velocities

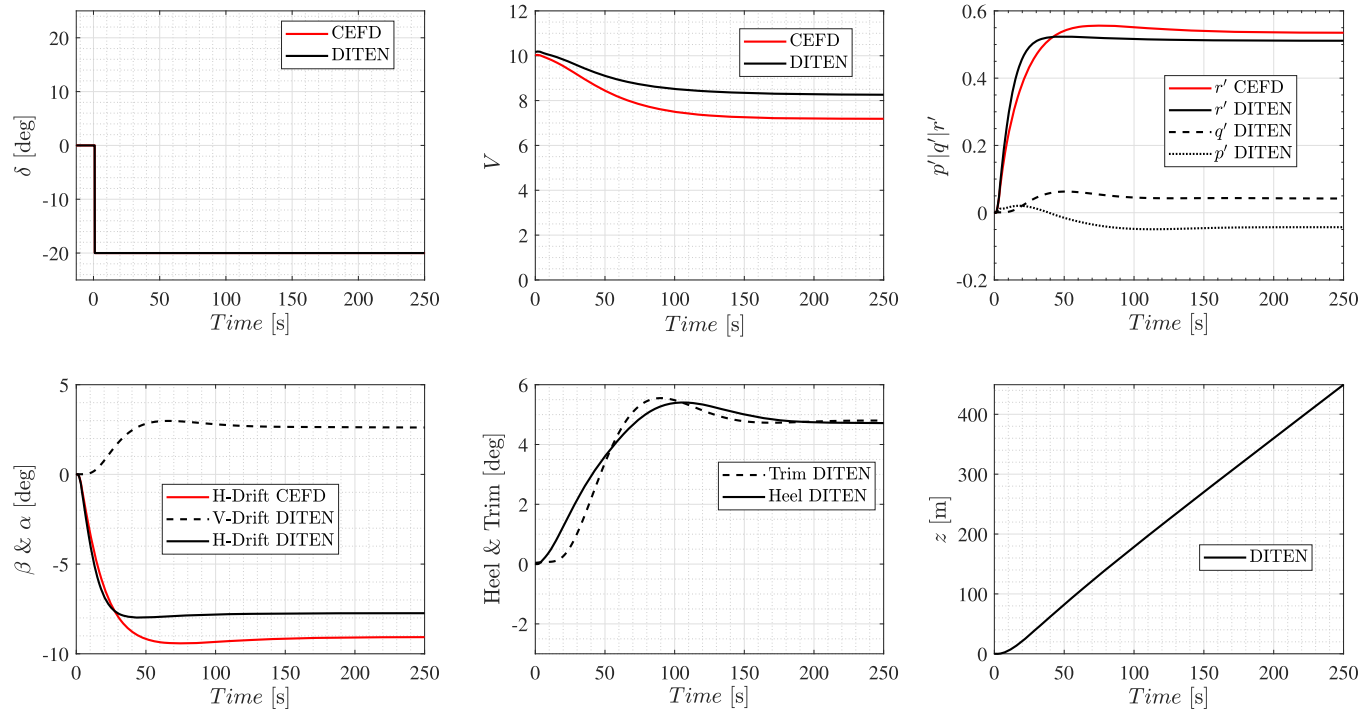

Fig. 33. BB2: turning circle 20° - principal parameters.

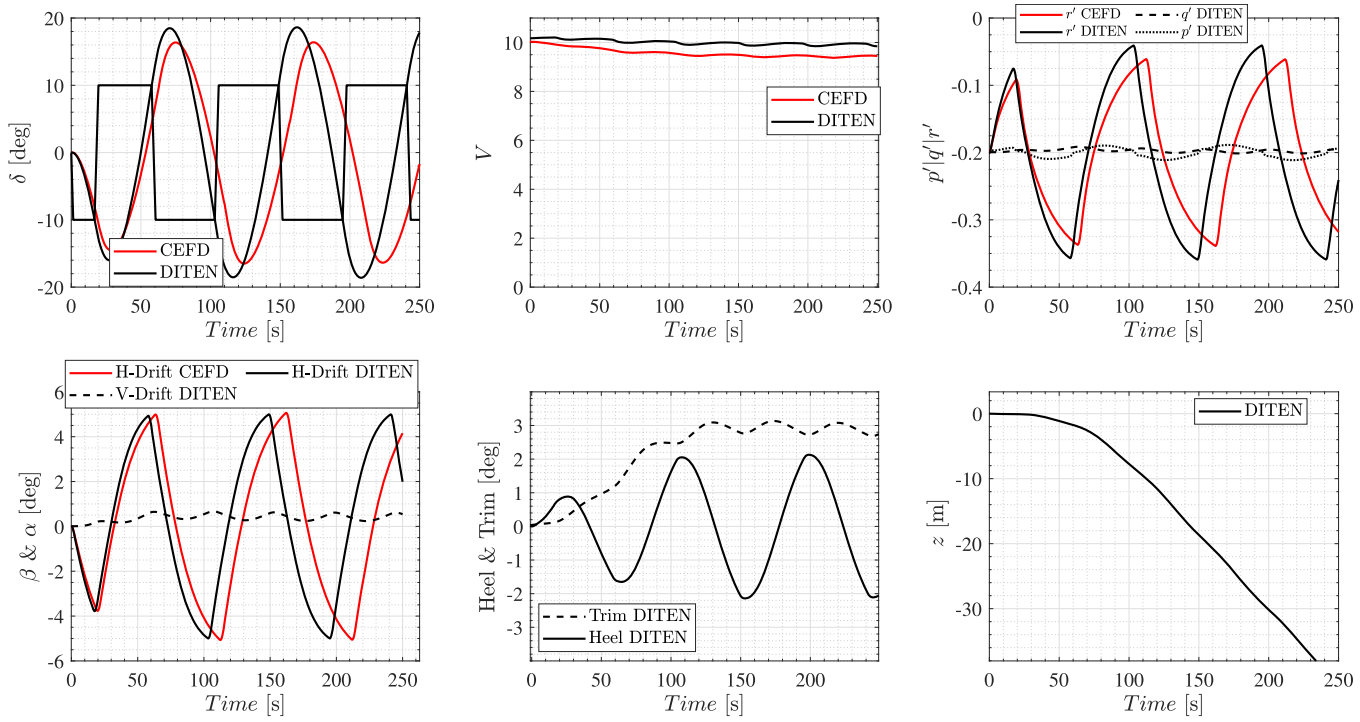

Fig. 34. BB2: horizontal zigzag 10-10 - principal parameters.

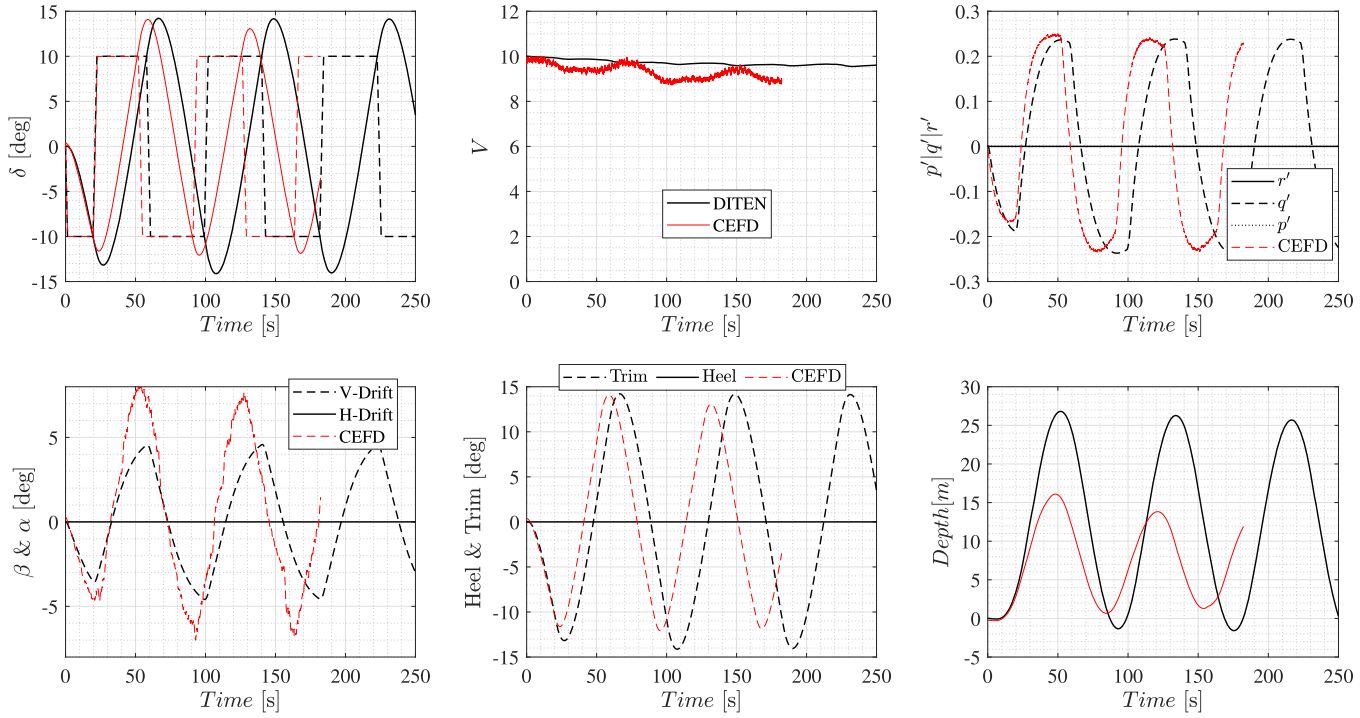

Fig. 35. BB2: vertical zigzag 10-10 - principal parameters.

in the horizontal plane (v and r), results are in rather good agreement, with an underestimation of drift angle. The main difference is observed in the speed drop, where specifically, the DITEN model tends to underestimate the speed drop by about 10 %.

Consistently the horizontal zig zag manoeuvre is well captured along the executions both in terms of overshoot angles and timings – see Fig. 34. All transient stages are well matched by the DITEN model.

Lastly, a coherent behaviour is found in terms of vertical zig zag – see Fig. 35. The zig-zag sequence is well captured, with the exception of an underestimation of the vertical drift angle by the DITEN model, which leads to a consistent overestimation of the explored depth range. As stated in the PMM analysis of Section 5.3, this will be the object of future works.

The analysis shown in the present paragraph does not add much information with respect to the previous one. It is clear that in general the

manoeuvres in the horizontal plane are sufficiently well captured, even if improvements may still be present. Also, the results in the vertical plane seem promising, even if requiring additional investigation. The only additional information is related to the necessity to analyse also the speed drop during the manoeuvres, which results underestimated as discussed.

Based on the overall trend of errors (Section 5.2) and the time-series analysis of the manoeuvres (Section 5.4), as well as the specific assessment of each test case, it can be concluded that the DITEN model provides a sufficiently reliable estimation of vessel manoeuvring performance. As such, it represents a potentially valuable tool at the design stage. This conclusion is further supported by the wide variation in parameters across the five test cases, including differences in main dimensions, types and extent of appendages, and stern plane configurations. Notably, the dataset includes a particularly unstable vessel, allowing the proposed model to be tested against a non-typical and challenging case. As observed, the code demonstrates greater robustness in the prediction of horizontal-plane manoeuvres, whereas discrepancies remain significant in the vertical plane, indicating the need for further investigation. This finding is also supported by the analysis of the PMM results (Section 5.3), which highlighted the necessity of improving the modelling of rudder stalling phenomena. Furthermore, the fourth subsection pointed to the need for additional analysis of resistance variations-and the consequent speed reduction-occurring during manoeuvres.

6. Conclusions

The present study has analysed and optimised various modelling approaches concerning the hull, sails, propellers, and control surfaces designs of submarines. The developed code has demonstrated a satisfactorily ability to simulate the dynamics of various submarines employing different designs of hull and appendages. In particular, when the SUBOFF is excluded from the mean absolute errors, the manoeuvring errors, expressed in terms of tactical diameters, are approximately around 0.3L. Specifically, for the 10° and 20° horizontal zig-zaag manoeuvres, the overshoot estimation error settled around 2° and 4°, respectively. In terms of vertical zig-zags, overshooting errors of 0.4° for the 5° manoeuvre and 1.2° for the 10° manoeuvre were observed. As reported in the previous section improvements can be expected especially for the vertical plane characteristics, then attention has to be given also to rudder forces (with particular care about stalling phenomena) and to added resistance during manoeuvres. For what regards manoeuvres in the vertical plane, as already indicated, it is important to remind that also experimental data are lacking, thus extending the requirement also to the enlargement of the experimental database.

It is believed, in general, that the models may be improved in future with the application of CFD to gain further insight into some physical phenomena, such as the interactions between appendages and main hull, stalling phenomena of the rudder, etc. These aspects will be object of future analyses.

In the meantime, it is believed that the proposed model may be already considered a sufficiently reliable tool for design purposes, especially when comparing the merits and shortcomings of different solutions and when analysing the global trend of systematic modifications of some characteristics (as some examples, comparison of X vs + configuration of stern planes, influence of the dimensions and location of appendages such as the sail.

CRediT authorship contribution statement

Lorenzo Berté: Writing – original draft, Visualization, Validation, Software, Resources, Methodology, Investigation, Funding acquisition, Formal analysis, Data curation; **Diego Villa:** Writing – review & editing, Visualization, Supervision, Data curation; **Michele Viviani:** Writing – review & editing, Visualization, Supervision, Software, Formal analysis, Data curation, Project administration; **Giorgio Mazzarello:** Writing – review & editing, Validation, Data curation; **Francesco Carmone:** Writing – review & editing, Data curation; **Benedetto Piaggio:** Writing – review & editing, Validation, Supervision, Software, Formal analysis, Data curation.

Declaration of competing interest

The authors declare that they have no known competing financial interests or personal relationships that could have appeared to influence the work reported in this paper.

Appendix A. CEFD model equations

$$\begin{aligned}X = {} & X_{qq}q^2 + X_{rr}r^2 + X_{rp}rp + X_{qIq}q|q| + X_{vrIr}vr|r| \\ & + X_{wqIq}wq|q| + X_{vr}vr + X_{wq}wq + X_{vv}v^2 + X_{ww}w^2 \\ & + X_{drdr}dr^2u^2 + X_{dsds}ds^2u^2 + X_{dbdb}db^2u^2 + X_{w}wu \\ & + X_{wIwI}w|w| + X_{drIdrI}dr|dr|u^2 + X_{ds}dsu^2 + X_{db}dbu^2 \\ & + X_{vw}wv + X_{vdr}vdru + X_{wds}wdsu + X_{wdsds}wds^2u \\ & + X_{wdb}wdbu + X_{vv\eta}v^2\eta + X_{ww\eta}w^2\eta \\ & + X_{drdr\eta}dr^2u^2\eta + X_{dsds\eta}ds^2u^2\eta.\end{aligned} \tag{A.1}$$

$$\begin{aligned}Y = {} & Y_{rIr}r|r| + Y_{pq}pq + Y_{pIpI}p|p| + Y_{rrdr}r^2dr + Y_{wrIr}wr|r| + Y_{qr}qr \\ & + Y_{r}ur + Y_{p}up + Y_{wp}wp + Y_{wr}wr + Y_{rdrIdrI}dr^2ru + Y_{\eta r}r\eta u \\ & + Y_{vq}qv + Y_{vIrI}\,\mathrm{sign}(v)\sqrt{v^2+w^2}|r| + Y_{rIvI}r\sqrt{v^2+w^2} \\ & + Y_{v}uv + Y_{vIvI}v\sqrt{v^2+w^2} + Y_{vw}vw + Y_{\star}u^2 \\ & + Y_{dr}u^2dr + Y_{drdrdr}u^2dr^3 + Y_{drIdrI}u^2dr|dr| + Y_{vdrdr}vudr^2 \\ & + Y_{vvdr}v^2dr + Y_{dreta}u^2dr\eta + Y_{v\eta}uv\eta + Y_{vIvI\eta}\sqrt{v^2+w^2}v\eta.\end{aligned} \tag{A.2}$$

$$\begin{aligned}Z = {} & Z_{rr}r^2 + Z_{pr}rp + Z_{pp}p^2 + Z_{qIq}q|q| + Z_{q}uq + Z_{vr}vr \\ & + Z_{IqIds}|q|dsu + Z_{vp}vp + Z_{wIqI}\,\mathrm{sign}(w)\sqrt{v^2+w^2}|q| \\ & + Z_{IwIq}\sqrt{v^2+w^2}q + Z_{q\eta}uq\eta + Z_{w}uw + Z_{vv}v^2 \\ & + Z_{\star}u^2 + Z_{ds}dsu^2 + Z_{dsdsds}ds^3u^2 + Z_{dsIdsI}ds|ds|u^2 \\ & + Z_{db}dbu^2 + Z_{dbdbdb}db^3u^2 + Z_{dbIdbI}db|db|u^2 \\ & + Z_{wdsds}wuds^2 + Z_{wwds}w^2ds + Z_{wdbdb}wdb^2u + Z_{wwdb}w^2db \\ & + Z_{dseta}u^2ds\eta + Z_{wIwI}w\sqrt{v^2+w^2} + Z_{vw}vw \\ & + Z_{w\eta}wu\eta + Z_{wIwI\eta}w\sqrt{v^2+w^2}\eta.\end{aligned} \tag{A.3}$$

$$\begin{aligned}K = {} & K_{pIpI}p|p| + K_{rIrI}r|r| + K_{qr}rq + K_{pq}pq \\ & + K_{p}up + K_{r}ur + K_{vq}qv + K_{wp}wp + K_{wr}rw \\ & + K_{v}vu + K_{vIvI}v\sqrt{v^2+w^2} + K_{vw}vw \\ & + K_{\star}u^2 + K_{\star}u^2\eta + K_{dr}u^2dr + K_{drIdrI}dr|dr|u^2 \\ & + K_{dreta}u^2dr\eta.\end{aligned} \tag{A.4}$$

$$\begin{aligned}N = {} & N_{rIrI}r|r| + N_{pq}pq + N_{qr}qr + N_{pIpI}p|p| \\ & + N_{r}ru + N_{p}pu + N_{wr}wr + N_{vq}qv + N_{rIvI}\sqrt{v^2+w^2}r \\ & + N_{wp}wp + N_{\eta r}u\eta r + N_{IrIdr}|r|dru \\ & + N_{\star}u^2 + N_{vw}vw + N_{vIvI}v\sqrt{v^2+w^2} + N_{v}vu \\ & + N_{dr}dru^2 + N_{drdrdr}u^2dr^3 + N_{drIdrI}dr|dr|u^2 \\ & + N_{vdrdr}vudr^2 + N_{vvdr}v^2dr + N_{v\eta}\eta uv \\ & + N_{vIvI\eta}v\sqrt{v^2+w^2}\eta + N_{dreta}u^2dr\eta\end{aligned} \tag{A.5}$$

$$
\begin{aligned}
\mathrm{M} = {} & M_{rr}r^2 + M_{pr}rp + M_{qIqI}q|q| + M_{pp}p^2 + M_q qu \\
& + M_{vp}pv + M_{vr}vr + M_{IqIds}|q|ds u + M_{q\eta}uq\eta D.L + M_{IwIq}\sqrt{v^2+w^2}q \\
& + M_w uw + M_\star u^2 + M_{vv}v^2 + M_{ds}ds u^2 + M_{dsdsds}ds^3u^2 \\
& + M_{dsIdsI}ds|ds|u^2 + M_{db}dbu^2 + M_{dbdbdb}db^3u^2 + M_{dbIdbI}db|db|u^2 \\
& + M_{wIwI}w\sqrt{v^2+w^2} + M_{wdsds}wds^2u + M_{\eta w}|w|u\eta \\
& + M_{wIwI\eta}w\sqrt{v^2+w^2}\eta + M_{vw}wv + M_{wwds}w^2ds \\
& + M_{wdbdb}wdb^2u + M_{wwdb}w^2db + M_{dseta}dsu^2\eta.
\end{aligned}
\tag{A.6}
$$

References

ABKOWITZ, M.A., 1964. Lectures on ship hydrodynamics-steering and maneuvering. Hydro Aerodyn. Lab. Rep. Hy-5. https://cir.nii.ac.jp/crid/1571417126341300992.

ABS, 2002. Rules for Building and Classing Underwater Vehicles, Systems, and Hyperbaric Facilities. American Bureau of Shipping.

Ankudinov, V., Kaplan, P., Jacobsen, B., 1993. Assessment and principal structure of the modular mathematical model for ship maneuverability predictions and real-time maneuvering simulation. In: Proceedings of the MARSIM'93, International Conference on Marine Simulation and Ship Manoeuvrability, International Marine Simulator Forum (IMSF). St. John's, NL, Canada. https://cir.nii.ac.jp/crid/1571135650717371648.

Bertè, L., Piaggio, B., Viviani, M., Villa, D., 2025. Development of a CFD-based submarine manoeuvrability prediction code. In: Proceedings of the 21st International Conference on Ship and Maritime Research (NAV 2025). Messina, Italy. Conference held from June 18 to June 20 2025.

Bohlmann, H.J., 1990. Berechnung Hydrodynamischer Koeffizienten Von Ubooten Zur Vorhersage Des Bewegungsverhaltens. Technische Universität Hamburg, Harburg, Germany.

Bridges, D.H., Blanton, J.N., Brewer, W.H., Park, J.T., 2003. Experimental investigation of the flow past a submarine at angle of drift. AIAA J. 41 (1), 71–81.

Carchen, A., Turkmen, S., Piaggio, B., Shi, W., Sasaki, N., Atlar, M., 2020. Investigation of the manoeuvrability characteristics of a gate rudder system using numerical, experimental, and full-scale techniques. Appl. Ocean Res. 106, 102419. https://doi.org/10.1016/j.apor.2020.102419

Clarke, D., 1972. A two-dimensional strip method for surface ship hull derivatives: comparison of theory with experiments on a segmented tanker model. J. Mech. Eng. Sci. 14, 53–61.

Dubbioso, G., Muscari, R., Di Mascio, A., 2013. Analysis of the performances of a marine propeller operating in oblique flow. Comput. Fluids 75, 86–102.

Feldman, J.P., 1979. DTNSRDC Revised Standard Equations of Motion. David Taylor Naval Ship Research and Development Center, Potomac, MD, USA. DTNSRDC/SPD-0393-09.

Feldman, J.P., 1995. Method of Performing Captive-Model Experiments to Predict the Stability and Control Characteristics of Submarines. Carderock Division Naval Surface Warfare Center, Bethesda, MD, USA. CRDKNSWC-HD-0393-25.

Gaggero, S., Piaggio, B., Vernengo, G., Villa, D., Viviani, M., Gualeni, P., 2022. Numerical approaches for submarine hydrodynamic design and performance analysis. Prog. Mar. Sci. Technol. 6, 279–286. 10.3233/PMST220035.

Gertler, M.H., Hagen, G.R., 1967. Standard equations of motion for submarine simulation. David W Taylor Nav. Ship Res. Dev. Center Bethesda MD, NSRDC-2510, 1–42.

Groves, N.C., Huang, T.T., Chang, M.S., 1989. Geometric characteristics of DARPA SUBOFF models (DTRC model nos. 5470 and 5471) .

Hooft, J.P., Nienhuis, U., Hutchison, B.L., Daidola, J.C., Jakobsen, B.K., Ankudinov, V., 1994. The prediction of the ship's maneuverability in the design stage. Trans. Soc. Naval Archit. Mar. Eng. 102, 419–445.

Joubert, P.N., 2004. Some aspects of submarine design part 1: hydrodynamics. Aust. Def. Sci. Technol. Organ. Report DSTO-TR-1622, 1–73.

Joubert, P.N., 2006. Some aspects of submarine design part 2: Shape of a submarine. Aust. Def. Sci. Technol. Organ. Report DSTO-TR-1920, 1–33.

Kim, D.-H., Kim, Y., Baek, H.-M., Choi, Y.-M., Kim, Y.J., Park, H., Yoon, H.K., Shin, J.-H., Lee, J., Chae, E.J., Shin, Y.-h., Kim, E.S., 2023. Experimental study of the hydrodynamic maneuvering coefficients for a BB2 generic submarine using the planar motion mechanism. Ocean Eng. 113428, 271.

Kirikbaş, O., Şakir, B., 2021. A review of the rules and regulations on submersible maneuvering. In: Proceedings of the 2nd International Congress on Ship and Marine Technology. Istanbul, Turkey, 2021.

Li, S., Liu, C., Chu, X., Zheng, M., Wang, Z., Kan, J., 2022. Ship maneuverability modeling and numerical prediction using CFD with body force propeller. Ocean Eng. 264, 112454. https://doi.org/10.1016/j.oceaneng.2022.112454

Liu, H.-L., Huang, T.T., 1998. Summary of DARPA SUBOFF experimental program data, 1–28.

Molland, A.F., Turnock, S., 2007. Marine Rudders and Control Surfaces Principles, Data, Design and Applications. Butterworth-Heinemann, Oxford, UK; Elsevier: Amsterdam, The Netherlands.

Munk, M., 1924. The Aerodynamic Forces on Airship Hulls. National Advisory Committee for Aeronautics. Report 184.

do Nascimento, C.E.G., Tannuri, E., 2020. Development of a submarine maneuvering simulator.

Ovalle, D.M., García, J., Periago, F., 2011. Analysis and numerical simulation of a nonlinear mathematical model for testing the manoeuvrability capabilities of a submarine. Nonlinear Anal. Real World Appl. 12 (3), 1654–1669.

Overpelt, B., Nienhuis, B., Anderson, B. Free running manoeuvring model tests on a modern generic SSK class submarine (BB2). In: Proceedings of the Pacific International Maritime Conference. Sydney, Australia.

Pattison, D.R., 1975. Stability and Control of Submarines: A Review of Design Criteria and Derivative Prediction Techniques. Procurement Executive Ministry of Defence, Haslar, UK. AEW Report no 7/75.

Perez, T., Fossen, T.I., Sorensen, A., 2004. A discussion about seakeeping and manoeuvring models for surface vessels. Centre Ships Ocean Struct. (CESOS), Tech. Report No. MSS-TR-001, 1–10.

Piaggio, B., Franceschi, A., Villa, D., Ferrari, V., Tonelli, R., Viviani, M., 2022a. The heel influence on ship manoeuvrability: single and twin-screw surface vessels. Ocean Eng. 266, 112721.

Piaggio, B., Vernengo, G., Ferrando, M., Mazzarello, G., Viviani, M., 2022b. Submarine manoeuvrability design: traditional cross-plane vs. x-plane configurations in intact and degraded conditions. J. Mar. Sci. Eng. 10 (12), 1–38.

Pitts, W.C., Nielsen, J.N., Kaattari, G.E., 1959. Lift and Center of Pressure of Wing-Body-Tail Combinations at Subsonic, Transonic, and Supersonic Speeds. National Advisory Committee for Aeronautics, Washington, USA. Report 1307.

Renilson, M., 2015. Submarine hydrodynamics. SpringerBriefs in Applied Sciences and Technology.

Renilson, M., Renilson, M., 2018. Manoeuvring and control. Submarine Hydrodynamics, 33–118.

Roddy, R.F., 1990. Investigation of the Stability and Control Characteristics of Several Configurations of the DARPA Suboff Model (DTRC Model 5470) from Captive-Model Experiments. David Taylor Research Center, Bethesda, MD, USA.

Spencer, J.B., 1968. Stability and control of submarines - Part I–IV. J. R. Nav. Sci. Ser. 23 (3), 187–205.

Sutulo, S., Moreira, L., Soares, C.G., 2002. Mathematical models for ship path prediction in manoeuvring simulation systems. Ocean Eng. 29, 1–19.

Thieme, H., 1965. Design of Ship Rudders. DTRC, Hamburg, Germany. Translation no.321, Original version "Zur Formgebung von Schiffsrudern" Schriftenreihe Schiffbau.

Thuné, S., 2015. Simulation of Submarine Manoeuvring. Master's thesis. Royal Institute of Technology Sweden. Stockholm, Sweden.

Toxopeus, S., 2008. Viscous-flow calculations for bare hull DARPA SUBOFF submarine at incidence. Int. Shipbuild. Prog. 55, 227–251.

Viviani, M., Martelli, M., Vignolo, S., Altosole, M., Figari, M., 2014. Numerical modelling of propulsion, control and ship motions in 6 degrees of freedom. Proc. Inst. Mech. Eng. Part M J. Eng. Marit. Environ. 228, 373–397.

Whicker, L.F., Fehlner, L.F., 1958. Free Stream Characteristics of a Family of Low Aspect Ratio Control Surfaces for Application to Ship Design. David Taylor Model Basin, Washington, DC, USA. DTMB Report 933.

Windsor, R.I., 1962. Survey of Low Aspect Ratio Characteristics Useful in the Design of Control Surfaces. University of Maryland, College Park, MD, USA. Wind Tunnel Report 62-1.

Yoshimura, Y., 2005. Mathematical Model for Manoeuvring Ship Motion (MMG Model). Technical Report.

Zheku, V.V., Villa, D., Piaggio, B., Gaggero, S., Viviani, M., 2023. Assessment of numerical captive model tests for underwater vehicles: the DARPA SUB-OFF test case. J. Mar. Sci. Eng. 11 (12), 2325.